Heliyon 10 (2024) e32157

Contents lists available at ScienceDirect

Heliyon

journal homepage: www.cell.com/heliyon

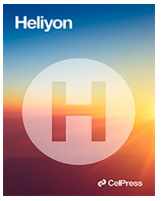

Review article

A review of simulation and numerical modeling of electric arc furnace (EAF) and its processes

Mahmoud Makki Abadi [a], Hongyan Tang [b], Mohammad Mehdi Rashidi [a,*]

[a] Institute of Fundamental and Frontier Sciences, University of Electronic Science and Technology of China, Chengdu, People's Republic of China
[b] School of Electronic Science and Engineering, University of Electronic Science and Technology of China, Chengdu, People's Republic of China

ARTICLE INFO

Keywords:
Electric arc furnace (EAF)
CFD simulation
Numerical modeling
Energy balance
Steel industry

ABSTRACT

Electric Arc Furnaces (EAFs) play a pivotal part in the steel industry, offering a versatile of producing high-quality steel. This paper conducts an in-depth examination of the EAF, along with exploring mathematical modeling and optimization techniques pertinent to this furnace. Additionally, it delves into the global steel production capacity employing this technology, introduces different processes associated with EAF, scrutinizes the energy balance of EAFs, and provides an overview of numerical and simulation modeling in this context. The core focus of this extensive review is the diverse landscape of EAF simulation methods. It places particular emphasis on understanding the key components and stages of the EAF process, including charging, melting, refining, tapping, and slag removal. The review delves into the wide array of approaches and methodologies employed in EAF modeling, spanning from innovative computational fluid dynamics (CFD) and finite element analysis to the intricacies of mathematical and thermodynamic models. Furthermore, the paper underscores the importance of simulation in predicting and enhancing crucial aspects such as heat transfer, chemical reactions, and fluid dynamics within the EAF. By doing so, it contributes to the optimization of energy efficacy and the ultimate quality of steel produced in these furnaces. In conclusion, this review identifies gaps in existing knowledge and offers valuable recommendations for improving mathematical process models, underscoring the continuous efforts to enhance the efficiency, sustainability, and environmental impact of steel production processes. In conclusion, several techniques aimed at enhancing both production rates and the quality of the melting process in EAF have been put forward.

1. Introduction

Steel, often hailed as the backbone of modern civilization, is the essential material that shapes our world. Its multifaceted applications in construction, infrastructure, machinery, and transportation are foundational to global progress [1,2]. Electric arc furnace (EAF) steelmaking is the manufacture of steel from direct reduced iron (DRI) or scrap melted by electric arcs. Now in the world, about 28.2 % of steel is produced by EAF, while in countries that do not have electricity problems, such as Iran, more than 90 % of steel in

Abbreviations: EAF, Electric Arc Furnace; CFD, Computational Fluid Dynamic; DRI, Direct Reduces Iron; DC-EAF, Direct Electric Arc Furnace; AC-EAF, Indirect Electric Arc Furnace; *S*C-EAF, Submerged Electric Arc Furnace; OHF, Open Hearth Furnace; BF-BOF, Blast Furnace-Basic Oxygen Furnace; SR-BOF, Smelting Reduction-Basic Oxygen Furnace; *S*C-EAF, Scrap-Based Electric Arc Furnace.

* Corresponding author.
E-mail address: mm_rashidi@yahoo.com (M.M. Rashidi).

https://doi.org/10.1016/j.heliyon.2024.e32157
Received 26 December 2023; Received in revised form 28 May 2024; Accepted 29 May 2024
Available online 31 May 2024

these countries is produced by this method [3,4]. The EAF has a molten bath and carbon electrodes are installed in its upper part [5,6]. Two materials, scrap and DRI, play the main role in the EAF, and failure to select the correct scrap in the melting operation can cause the electrodes to break or the molten steel to fall [7,8]. Nowadays, it is feasible to charge as hot direct reduces iron (H-DRI), hot metal and pig iron. Ferroalloys include different alloys of iron and are added to steel to achieve a specific chemical composition. Ferrocarbons are considered to be very strong depletes oxygen and are used in direct arc furnaces [9].

The EAF is divided into three types, direct electric arc furnace (DC-EAF) and indirect electric arc furnace (AC-EAF), and submerged electric arc furnace (*S*C-EAF) based on the passage of electric current [10,11]. (i) DC-EAF [12–15]. Recently, several researches studied to model and simulate electric arc blinds using different software such as FLUENT, ANSYS and COMSOL [16–20]. Also, in other researches, the calculations of conservation of mass and energy [21], chemical equations in EAF [22], governing equations of radiant heat transfer [23], displacement and mass transfer [24], as well as the magnetic field were created on melt, DRI and slag, and their codes were written by different software such as MATLAB and FORTRAN [25,26] and use building statically models. Several researchers have delved into the intricate procedure of a plasma curve interacting with a melted soak using mathematical simulations within a direct current-electric arc furnace (DC-EAF) [27,28]. Experimental measurements on the speed field and the turbulent electromagnetically-driven movement in the presence of DC-EAF current were reported by Murthy et al. [29]. Some investigators concentrated solely on modeling the plasma arc, disregarding the presence of the melted soak [30,31]. Meanwhile, others directed their efforts toward emerging representations for the melted soak, omitting considerations for the plasma arc [32–35]. Considering that EAF slag improves the mechanical performance and durability of mixtures as well as their long-term stability, it is important to simulate slag and other chemical reactions in EAF [36–38].

Khodabandeh et al. [39] provided a summary of parametric study of heat transfer in an electric arc furnace and cooling system. Their result showed that the effects of slag layer thickness on the walls were also numerically investigated and it was observed that the formation of slag layer on the furnace walls has a significant impact on the safe operation of the furnace and improved furnace efficiency. Reynolds [40] introduced a radiation model designed for electric arc furnaces used in smelting. This model indicates that the primary source of energy loss is radiation from the surface of the molten bath, rather than the plasma arc column. Li et al. [41] established a 3D reproduction model to simulate flat-bath circumstances within the freeboard of an alternating current (AC) electric arc furnace (EAF). A review of Electric Arc Furnace (EAF) modeling and simulation was conducted by Vinayaka and Puttaswamy [42]. Several EAF models were modeled and reviewed from power quality assessment. Voltage flicker, Harmonics and Inter harmonics arises in an electrical network due to the non-linear nature of EAF operation.

Daneshmand and Heydari [43] explored the use of TiO_2/SiC coating on graphite electrodes in EAF to reduce electrode corrosion. Their approach involved a combination of numerical simulations, experimental methods, and industrial testing within the EAF. In a study by Makrygiannis et al. [44], the impact of electrode form, electrode involvement depth, and slag thermal conductivity on the heating effectiveness of EAF in ferronickel dispensation was investigated using a 2D steady-state model. Zhang et al. [45] planned a mathematical model to examine the multi-physical arena circulation in EAF during the melting procedure of CaC_2. Yu et al. [46] developed a 3D mathematical model separated into the arc zone and ore zone to study the passing heating procedure of ores in the flooded AC-EAF for ferrochrome melting. A combination of several optimization algorithms of the EAF is utilized to solve the optimization problem was studied by Saboohi et al [47]. Their results show that optimized operation profiles lead to a significant decrease in operational costs and production times. Optimization-based online decision provision instrument for EAF process was analyzed by Shyamal et al. [48]. Their report was advanced utilizing completely open-source utensils to consume a high petition to industrial consultants.

As the paper progresses, it identifies existing gaps in knowledge, paving the way for future developments and refinements in mathematical process models. In an era where the steel industry is at a crossroads, balancing the need for increased production with the necessity for environmental responsibility, this review stands as a cornerstone resource for researchers, engineers, and stakeholders. The objectives of this paper can be followed as an introduction to EAF. Also, in this paper, it has been tried to provide the necessary information about energy consumption, the type of operation of EAF, the different stages of EAF, and also a summary of furnace simulation in recent years. It provides invaluable insights into the current state of EAF simulation and sets the stage for continued advancements in this critical domain. Also, in this paper, some important points to enhance the production of the EAF system will be presented.

2. Literature review

In this part, various approaches to the modeling of EAF process have been explored in literature to better understand and optimize its operation. Mathematical models play a crucial role in understanding and optimizing the complex processes involved in EAF operation. Here, distinct groups based on the various modeling approaches of the EAF. These approaches can be broadly categorized into thermodynamics-based models, data-driven models and hybrid models.

Thermodynamics-based models aim to simulate the physical and chemical processes within AF using fundamental principles of the thermodynamics. Matson and Ramtirez elaborated on one of the earliest models of the entire EAF process [49,50], wherein the furnace was divided into two control volumes: (1) a gas control volume and (2) a control volume comprising the slag and bath. The melting model incorporated partial differential equations to compute changes in scrap temperature and melting rates based on sensible heat and latent heat of fusion. Nyssen et al. [51] developed a numerical EAF model consisting of 15 sectors. Every sector exhibits a unique melting rate based on its position within the furnace and has specific layers of scrap. Ten modules were identified to describe the physical components of the furnace, including scrap, liquid metal, slag, solidified metal, refractory lining, arc, furnace chamber exhaust gas system, burners, and roof and panels modules. Modigell et al. [50] explored an EAF model designed as a simulation tool.

The modeling comprised four zones: molten metal, scrap, metal-slag, and post-combustion. The scrap zone primarily contained the scrap, while the slag metal zone encompassed the slag phase and a portion of the metal path. Chemical equilibrium was presumed within these zones due to the high temperatures, which ensured that they were not constrained by reaction kinetics. They verified their model by comparing it with the off-gas composition and end-point measurements, which included the final bath chemistry as well as the masses of steel, slag, and off-gas. In contrast to the comprehensive EAF models discussed earlier, Guo and Irons [52] created a three-dimensional radiation model to assess the distribution of radiative energy within the furnace. The model utilized the power factor, current, and voltage to quantify the energy emitted by the arc.

Data-driven models utilize empirical data to develop predictive algorithms for EAF operation. Andonnovski and Tomazic [53] conducted a comparative analysis of data-driven models for forecasting and optimizing energy usage in EAF. During the modeling phase, they emphasized the advancement of fuzzy modeling techniques in contrast to several established machine learning approaches. Tomazic et al. [54] introduced a data-driven modeling and optimization approach for managing energy consumption in EAF operations. The study outlines four distinct modeling methodologies aimed at predicting electrical energy usage during EAF processes: linear regression, k-NN modeling, evolving fuzzy modeling, and conventional fuzzy modeling. During the learning phase, a subset of significant repressors impacting energy consumption was selected from a pool of over ten candidates. Validation and comparison of all models, using 30 % of the available data, revealed the fuzzy model's notable accuracy in predicting energy consumption. Implementation of these models is anticipated to result in reduced energy consumption and improved efficiency of EAF operations. Manojlovic et al. [55] conducted a study on the machine learning analysis of the electric arc furnace process to assess energy efficiency parameters.

Hybrid models combine elements of both thermodynamics-based and data-driven approaches to improve predictive accuracy and computational efficiency. Hernandez et al. [56] introduced an industrial EAF model that integrated several rigorous first-principles sub models of heat exchange within the EAF, coupled with practical insights from an operational melt shop. They posited that the energy requirements of the process are met by six sources, including the electric arc, oxy-fuel burners, oxygen lances, coal combustion, and metal oxidation in both liquid and solid phases.

A review of mathematical process models for the electric arc furnace process was conducted by Hay et al. [57]. This paper reviews mathematical process models proposed in the literature, identifying the most common modeling approaches, and uses mathematical descriptions for the main phenomena. In addition to first principles-based models, empirical modeling approaches have also been widely employed to capture the complex behavior of EAFs. These models are often derived from experimental data to correlate input parameters such as material composition, operating conditions and electrode position with output variables like chemical compositions of the melt and energy consumption.

Some researchers utilize machine learning techniques to streamline the modeling of intricate phenomena like the electric arc. Within this category, artificial neural networks are employed to estimate arc length [58,59], while others are trained to directly replicate measurement data [60–62]. Klimas and Grabowski [63] explored an EAF modeling approach rooted in deterministic differential equations but enriched with stochastic elements. Their modeling efforts were twofold: first focusing on melting stage measurement data, and then on the refining stage. Ruiz et al. [64] explored machine learning techniques for predicting the inclusion content in clean steel produced through electric arc furnace and rolling processes. Several findings from their investigation were deemed valuable for integration into steel manufacturing practices. Choi and et al. [65] conducted research on a machine learning-driven project aimed at predicting and controlling tap temperature to optimize power consumption in stainless steel electric

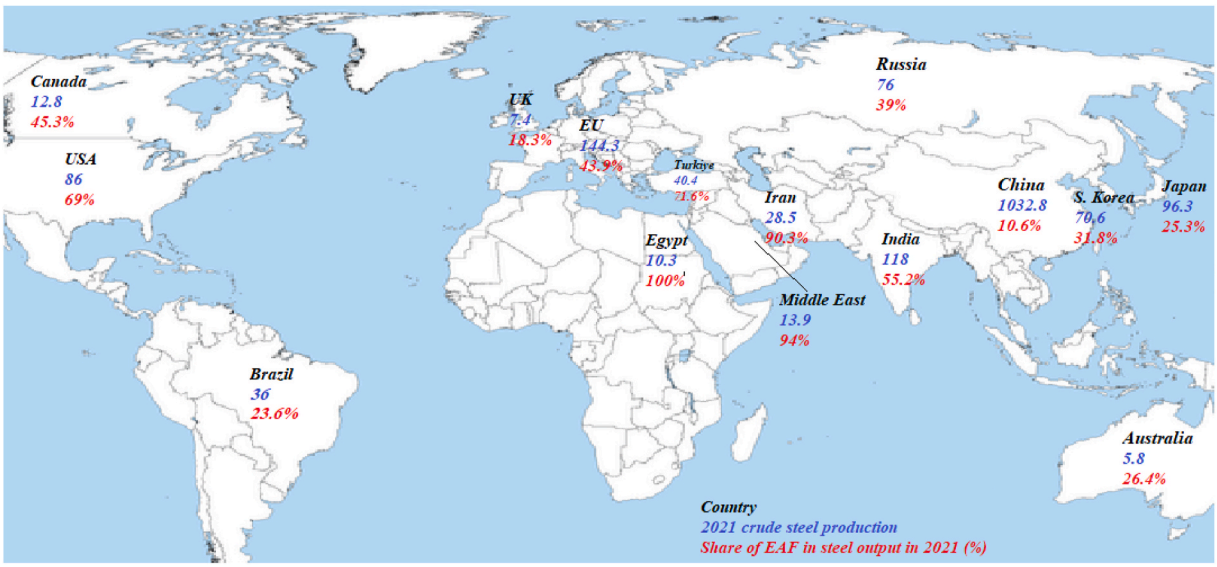

Fig. 1. Total steel production as well as the percentage of technology EAF-DRI steel production for countries in 2021 [66].

arc furnaces at steel plants. Their economic evaluation of the facility investment revealed satisfactory economic feasibility, with an internal rate of return (IRR) of 35.8 %.

3. EAF capacity in the world

According to Worldsteel data [66], the global share of steel production via EAF increased from 25 % to 29 % between 2015 and 2021, with electric steel output rising by over 150 million tons during this period. Consequently, the demand for scrap surged by approximately 170 million tons, marking a 37 % increase over the past six years. Presently, new steel capacity projects, either underway or announced, predominantly rely on EAF technology. Even initiatives focused on direct reduction iron (DRI), considered a leading green technology in the steel industry, incorporate electric furnace steel production. Notably, all EAFs within DRI projects are hybrid furnaces, facilitating the utilization of DR pellets or scrap in varying proportions as raw materials. Consequently, DRI projects are expected to further drive the utilization of scrap materials.

In various regions, steel production has witnessed significant electrification. Notably, the Middle East stands out with nearly 95 % of its steel capacities being electric steel mills, followed by Turkiye and USMCA countries (USA, Canada, and Mexico) with approximately 70 %. Although China (China now produces about 10 % of its steel with technology EAF (has been slower in this transition, its evolving dynamics and future plans are poised to have a substantial impact on the global scrap sector. The worldwide utilization of ferrous scrap witnessed a notable uptick in 2021, rising by 12 % to reach 620 million tons, signifying a substantial surge within the scrap industry. This surge can be attributed to the industry's inherent characteristics, wherein the supply is relatively rigid, unable to promptly adjust to meet fluctuating demand. The total steel production as well as the percentage of technology EAF-DRI steel production for each country in 2021 is shown in Fig. 1. The countries of Egypt (100 %), Iran (over 90 %), Middle East (over 94 %) and USA (more than 69 %) produce most of their steel production with technology EAF. Also, about 43 % of steel in European countries is produced with technology EAF.

4. Electric arc furnace (EAF)

An electric arc furnace is a highly heated, enclosed environment designed for metal melting through electrical arcing, while preserving the metal's electrochemical properties. These furnaces operate at elevated temperatures and rely on high-voltage electric current as their main component, creating an electric arc between the electrodes to facilitate the metal's melting process. There are mainly three types of electric arc furnaces [67–69].

- Direct electric arc furnace (DC)
- Indirect electric arc furnace (AC)
- Submerged electric arc furnace (SC)

In a direct electric arc furnace, the arc is established between the electrodes and the material to be heated. This furnace type

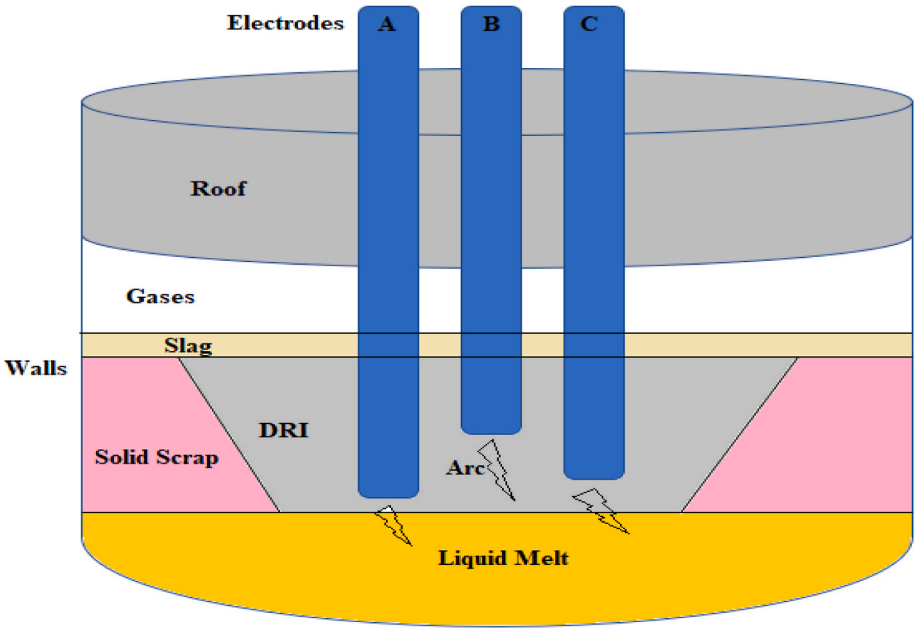

Fig. 2. Electronic arc furnace.

employs two carbon or graphite electrodes, and the arc originates at two locations: between the electrodes and the charge. This heating method enables the attainment of high temperatures because the arc is generated directly within the charge to be heated. Additionally, there is extra heat generated within the charge due to the passage of electrical current. In a single-phase arc furnace, two electrodes are vertically inserted from the furnace's top into the charge. Conversely, in a three-phase arc furnace, three electrodes are positioned at the corners of an equilateral triangle, resulting in the formation of three arcs and creating a star configuration. In an indirect electric arc furnace, the arc is created between two electrodes positioned near the charge, and the heat generated by the arc is then moved to the charge primarily through radiation. The formation of the arc involves briefly bringing the electrodes into contact and then retracting them. Since the arc doesn't have direct contact with the charge, the temperature achieved in an indirect arc furnace is typically lower than in a direct arc furnace. These furnaces are usually single-phase and are of limited size. Indirect electric arc furnaces are commonly used for processes like melting nonferrous metals and in iron foundries where the goal is to produce molten metal [70–72]. The operational principles of an electric arc furnace involve a sequence of steps including entering the electrode, melting the metal, and refining. Initially, the heavy and light scrap materials in the receptacle are preheated using exhaust gas. Burnt lime and spar are introduced to facilitate the rapid formation of slag. The electrodes are then gradually lowered into the scrap, leading to the generation of an electric arc between the electrode and the metal. Initially, a low voltage is employed, and once the arc is sufficiently protected by the electrodes, the voltage is augmented to expedite the melting procedure [73–75]. Electric arc furnaces are basically a large, shallow bath with a steel body; which are covered with heat-resistant refractory materials [76]. Also, the temperature in these furnaces is very high (about 3000 °C) and almost no non-combustible material can withstand such a temperature. For this reason, to reduce the temperature, the body and roof of these furnaces are covered with water pipes. In general, the body of electric arc furnaces consists of three main parts, which are: floor or bush (heats), side wall (shell) and roof (roof). (i) Roof: it is in the form of a cap and is usually designed in such a way that it is both light and has the necessary strength. There are usually three holes in the roof of electric arc furnaces, and these three holes are where the electrodes pass. In electric arc furnaces, the roof is usually designed to be movable along with the electrodes. (ii) Shell: They are generally cylindrical and covered with refractory materials as well as water pipes. (iii) Heats: it has an arched shape, and unlike the roof, its depth is relatively low and its surface is high, so that the interface between the

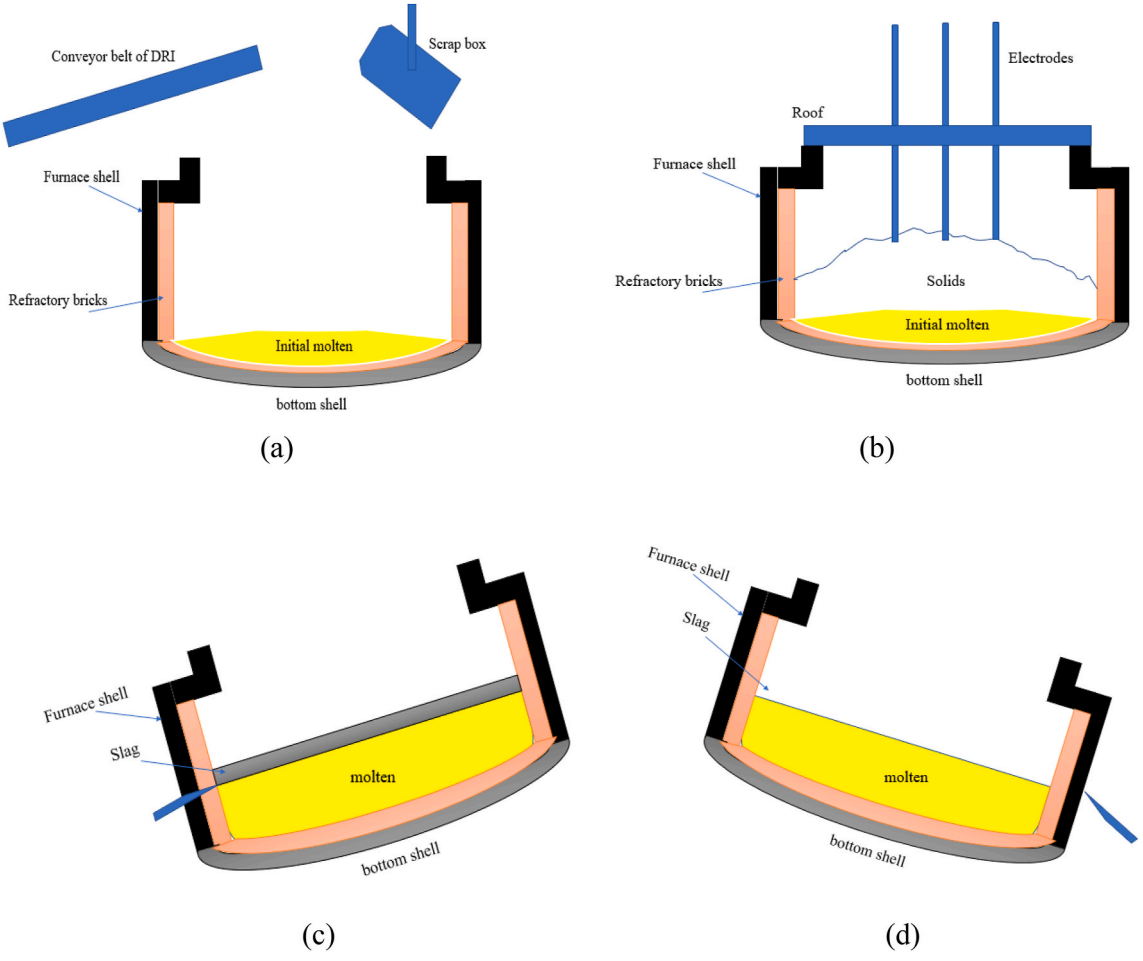

Fig. 3. Processes in EAF
(a) Charging process, (b) Melting process, (c) Slag removal process, and (d): Tapping process.

melt and the slag is the largest [77,78]. A general schematic of the EAF is shown in Fig. 2.

4.1. Processes of EAF

The Electric Arc Furnace (EAF) functions in a batch melting mode, creating consignments of liquid steel. The entire tap-to-tap cycle of the EAF comprises several sequential stages, including (i) charging (DRI and scrap) in the furnace, (ii) melting, (iii) refining, (iv), (v) slag removal, (vi) tap out, and (vii) turning around the furnace for the next cycle [77–81]. In today's EAF operations, there is a strong emphasis on achieving tap-to-tap times of under 60 min, and some EAFs employing twin shells have successfully reduced this time to approximately 35–40 min [82–84]. This increased efficiency in the steelmaking process is a notable development in modern EAF operations.

4.1.1. Charging (DRI and scrap)

In the charging step of an (EAF), a combination DRI and scrap steel is loaded into the furnace. Generally, DRI is deposited into EAF by a conveyor belt and scrap iron by a metal box. The ratio of DRI to scrap steel utilized during charging can be adjusted based on the specific steel production needs, the desired steel composition, and the accessibility of these resources. The charging phase plays a critical role in shaping the ultimate composition of the molten steel created within the EAF. This step is integral to the steelmaking process, facilitating effective recycling and the manufacture of top-notch steel products. Casting of sponge iron is done with a conveyor belt. The height of the conveyor belt should be determined so that the sponge iron can easily pass through the slag. The scraps should place in the bucket as said by their size and density to rapidly form a liquid pool of steel inside the furnace while protecting the side walls and roof against the radiation of the electric arc. The charging process can be observed in Fig. 3-a.

4.1.2. Melting

The melting step within the EAF is a dynamic and meticulously managed procedure that transforms solid substances into a scorching, liquefied steel pool. The melting process can be detected in Fig. 3-b. The effectiveness of this phase profoundly influences the ultimate quality and constitution of the manufactured steel, rendering it an indispensable facet in contemporary steel production. Electricity is the primary energy source, introduced through graphite electrodes, and plays a significant role in the melting operation. The EAF operates by using powerful electric arcs to generate intense heat. These arcs are created between the tips of large, graphite electrodes and the charged materials within the furnace. Electrical current passes through the scrap and other materials, generating extreme temperatures up to 3000 °C. Initially, a lower voltage tap is used until the electrodes penetrate the scrap material. Lighter scrap is often positioned on top to expedite this penetration process.

4.1.3. Refining

The refining phase in the EAF is a pivotal stage where the chemical composition and temperature of the melted steel are meticulously controlled and fine-tuned to satisfy precise quality and performance criteria. The refining process in the EAF aimed at eliminating slags like phosphorus, sulfur, aluminum, silicon, manganese, and carbon from the steel. Totally, temperature control, chemical composition adjustment, removal on non-metallic inclusions, homogenization, gas removal and final temperature adjustment are main tasks in refining step in EAF. However, recent advancements in our understanding of dissolved gases, particularly hydrogen and nitrogen, have highlighted the necessity of regulating these gases to acceptable levels. It's worth noting that once a flat bath is achieved during refining, these gases are not typically removed. Oxygen remains present in the bath during the flat bath operation to reduce the carbon content to the desired level for tapping. Most of the compounds targeted for removal throughout refining exhibit a stronger attraction to oxygen than carbon. Consequently, oxygen selectively responds with these elements, forming oxides that then rise to the surface of the steel and are carried away by the slag. In modern EAF processes, particularly those that maintain a "hot charge" of molten steel and retained slag from the previous heat, oxygen is frequently introduced into the bath during the process. This innovative approach enables the simultaneous execution of both smelting and refining operations within the furnace [85,86]. Elkoumy et at [87]. studied the empirical model for predicting process parameters during EAF refining stage based on real measurements. Their studied parameters were steel melt carbon content and temperature. High temperature investigations with temperature of 1550–1700 °C with different chemistry ranges and mainly carbon content with 0.02–0.2 % C were done during the refining stage operation. Their results showed that the refining stage takes place in about 3–7min. and consumes 4%–12 % of the total energy consumed through the whole EAF batch process and the specific electrical energy consumption during EAF refining stage can be calculated with the following equations:

$$EAF\ epecific\ electrical\ redining\ energy\left(\frac{kWh}{ton}\right) = -1.77 + 8.8 + Refining\ PON(\min) + 1.07 * Specific\ refining\ oxygen\left(\frac{nm^3O_2}{ton}\right) - 0.33 * specific\ refining\ carbon\ injection\left(\frac{kg}{ton}\right) + 0.404 * specific\ refining\ lime\ injection\left(\frac{kg}{ton}\right) \quad (1)$$

It has been shown that the metallic yield for 50 % DRI charge containing oxidized DRI with low metallization of 80%–85 %, 78%–82 % metallic iron" and low-carbon content of 1.2%–1.4 % C can be improved from 78.1 % to 88.8 % by increasing the specific carbon addition from 25.3 to 43.1 kg carbon ton^{-1} molten steel. It was found that the steel melt flow velocity increases by a combined effect of the steel melt temperature and composition, and slag pressure [88,89].

4.1.4. Slag removal

The process of extracting slag from an EAF is a crucial stage in contemporary steel production, with the primary purpose of eradicating unwanted impurities and non-metallic elements from the molten steel to attain the desired quality and composition. Slag, generated as a byproduct in the steelmaking procedure, comprises diverse non-metallic elements like oxides, fluxes, and impurities. The elimination of this slag is indispensable since it plays a key character in preserving the integrity and purity of the ultimate steel product [90]. The slag removal process can be observed in Fig. 3-c. Slag is formed during the EAF process due to the chemical reactions between the steelmaking raw materials and the impurities present in the scrap steel, DRI, or other materials charged into the furnace. Once the slag has been extracted from the EAF, it is usually directed into a slag pot or a designated container. This slag container is designed to withstand the high temperatures and the corrosive nature of the slag. It can be moved away from the furnace area for further processing.

4.1.5. Tapping

During the tapping phase of an EAF, the final, refined molten steel is drawn from the furnace, marking a pivotal stage in the steelmaking cycle. This transition point signifies the readiness of the molten steel to be shaped into various forms for subsequent processing and applications. Lance insertion and sampling (prior to tapping, this lance typically incorporates a temperature-sensing device to monitor the steel's temperature), final adjustments (any last-minute modifications to the steel's composition or temperature can be implemented), tapping aperture, tapping procedure (the molten steel gracefully exits the furnace through the tapping orifice, streaming into a ladle or another designated receptacle) are main parts in tapping steps in EAF process. The tapping process for EAF is shown in Fig. 3-d.

4.2. Energy consumption of EAF

The consumption of electricity, natural gas, and water in an EAF can vary depending on several factors, including the furnace's size, configuration, and operating conditions. The overall energy intensities observed in the examined EAFs varied between 510 kWh/t and 880 kWh/t [79] (see Fig. 4). Enhancing energy efficiency entails reducing energy losses to the EAF off-gas and water-cooling systems. A schematic of input and output energies in a EAF is shown in Fig. 4.

Considering the electricity consumption of EAF is high, extensive studies have been done on the energy intensity of EAF in recent system. A case study of energy intensity of steel manufactured utilizing EAF technology in Poland in the years 2000–2019 was investigated by Gajdzik et al. [81]. Their analysis was done in accordance with the methodology of building statistical models. In their study, a research hypothesis was developed concerning the correlation between the volume of steel production through the EAF method and the energy consumption associated with the process. Carmona et al. [82] conducted an analysis of the UK's steel industry

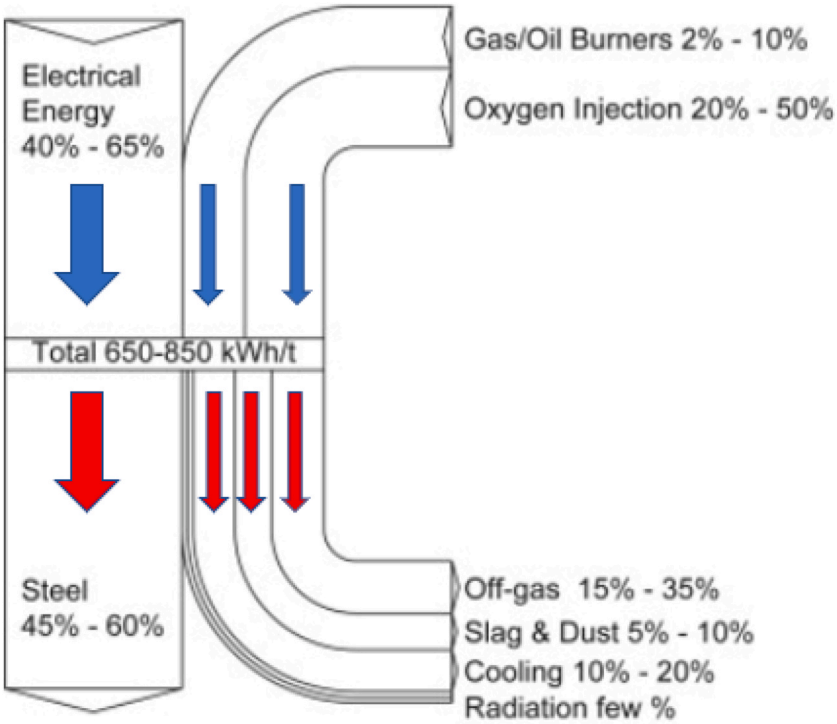

Fig. 4. Energy sources in an EAF (e.g., electrical energy and chemical energy resulting from oxidation reactions) and energy sinks (e.g., off-gas extraction and furnace cooling systems) [79].

spanning from 1960 to 2009. The study focused on assessing "resource efficiency" and "useful exergy efficiency" concerning both the BF + BOF and EAF technologies. The findings revealed an overall increase in the sector's resource efficiency from 19 % to 32 % during this period. Specifically, the resource efficiency of the BOF route increased by 9 %, while the EAF route saw a more substantial rise of 20 %. Similarly, in their examination of the Indian steel sector, Dasgupta & Roy [91] noted a decline in energy intensity from 41.9 GJ/tonne of steel in 1990 to 27.3 GJ/tonne in 2008. However, this figure remained higher compared to energy intensities observed in the USA (14.90 GJ/tonne) and China (23.11 GJ/tonne). Conversely, research by Wiboonchutikula et al. [90] in Thailand yielded different outcomes. Despite the generally lower energy intensity of the EAF technology, the BF + BOF route is projected to maintain dominance in many emerging countries.

4.3. Energy balance of EAF

An energy balance in an EAF is a fundamental concept used to track and assess the distribution of energy within the furnace during the steelmaking process. It helps in understanding how energy is utilized and lost at various stages, ultimately influencing the furnace's efficiency, performance, and steel quality. As shown in Fig. 5, about 1038 kg scrap iron is wanted to harvest 1 ton of iron using EAF. If its main feed is DRI, about 1200 kg of DRI is wanted to harvest 1 ton of iron. The input amount of lime, carbon, natural gas and oxygen is equivalent to 28, 21, 4 and 56 kg/ton, respectively. If only scrap iron is used, the amount of slag output is equal to 78 kg, and if the input feed is sponge iron, the amount of slag produced will be equal to 205 kg. The quantity of effort and production materials for the making of 1 ton of steel in the two cases of using scrap iron (red line) and DRI (black line) is shown in Fig. 5 [80].

5. Numerical modeling and CFD simulation of EAF

The aim of this section is to the present comprehension of the EAF process is still not fully comprehensive, primarily owing to its intricate nature and the extremely challenging operational environments. While CFD models have been constructed to delve into specific furnace sections and are ideal for design and engineering analysis, their extended simulation times make them unsuitable for real-time control applications. Previous modeling efforts aimed at simulating industrial EAF processes have often involved simplifying assumptions and a division of the furnace into multiple zones to facilitate analysis [92–94]. The heat and mass transfer within and amid the various regions are labelled utilizing suitable mathematical equations. In a dynamic EAF model projected in Ref. [95], there are four steadiness regions with mass transport limits (as can been see Fig. 6): the gas region, slag-metal interaction region, melted steel region, and solid scrap region.

1. The gas zone contains gases like O_2, CH_4, CO, CO_2, H_2, and N_2, which fill the free-board capacity upstairs the steel scrap.
2. The slag-metal interaction zone comprises slag materials and the upper part of molten metal in contact with the slag. It includes elements like C, CO, Al, Fe, FeO, SiO_2, and MnO.
3. The solid scrap zone consists of the remaining solid scrap steel.

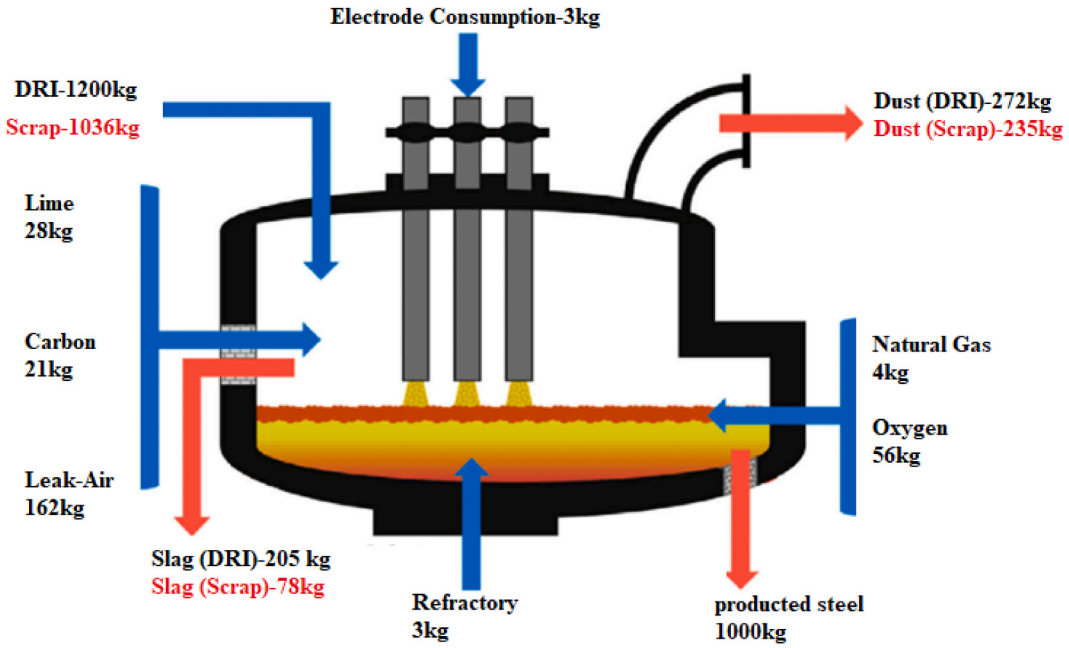

Fig. 5. Energy balance for EAF (Scrap and DRI) [80].

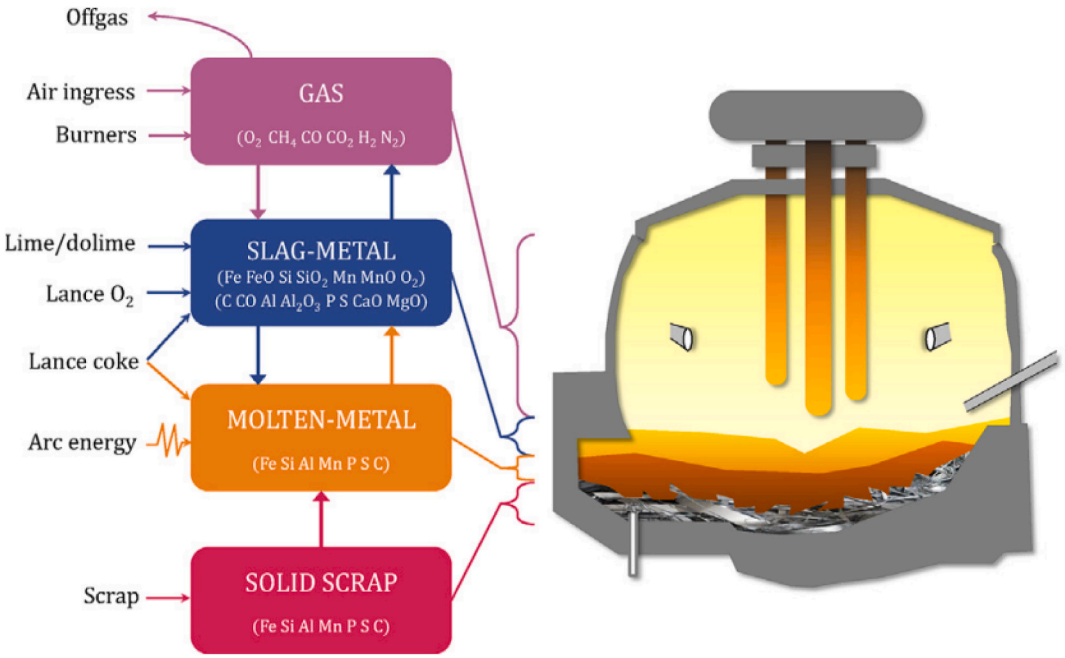

Fig. 6. Schematic of EAF model with gases and material in each region [84,92].

This approach offers the advantage of requiring fewer parameters compared to a model according to reaction kinetics. Shyamal et al. [96] conducted a study on real-time energy organization for EAF process, showing that optimal input decisions can be made with adequate computational rapidity for real-time application.

Consequence of arc length on fluid flow and socializing singularities in AC-EAF was studied by Gonzalez et al. [97]. Some assumptions that are made in this paper as following.

- The entire computational domain is filled with liquid steel, and the model does not consider the presence of the top slag stage or the formation of CO.
- The furnace walls are assumed to be at a continuous temperature of 1500 °C, which is nearby to the liquidus temperature of low-carbon steels.
- The model does not account for radiation from the walls and roof.
- It operates under steady-state conditions.
- The pouring forces are primarily buoyancy forces, with Marangoni forces being neglected.
- Electromagnetic forces are not considered for an AC-EAF.
- Rousing resulting from oxygen inoculation or bottom gas injection is not comprised in the model.

A schematic of Furnace AC-EAF designed and modeled by Gonzalez et al. is shown in Fig. 7. As it is known, the dimensions of the cross section of the furnace are 6700 * 7710 mm and the type of furnace is AC that there were three electrodes in this simulation.

The governing equations are conservation of energy, momentum, and mass. These equations can be summarized by the succeeding

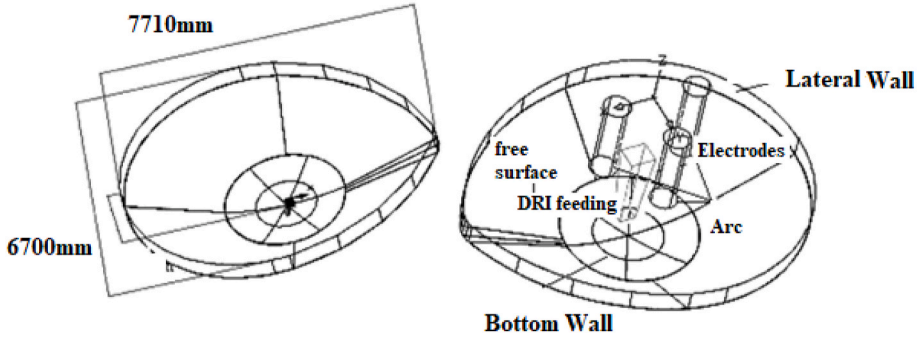

Fig. 7. Computational domain [93].

general appearance [97]:

$$\nabla.D\nabla\varnothing - \nabla.(\rho V\varnothing) + S = \frac{\partial\rho\varnothing}{\partial t}, \tag{2}$$

where ∅, D, and S are reliant on adjustable (for instance: velocity and temperature), diffusion coefficient in kg/m.s and basis term(s) diverse to convective, diffusive or transient terms, respectively.

Also, for mass conservation for a fluid of constant density [97]:

$$\nabla.v = 0, \tag{3}$$

where v signifies the velocity vector.

For thermal energy conservation in EAF, this equation can be followed [97]:

$$\nabla.\frac{k}{C_P}\nabla\mathrm{T} - \nabla.(\rho vT) = \rho\frac{\partial T}{\partial t}, \tag{4}$$

where, k, C_P and ρ signify thermal conductivity, heat capacity and density of liquid steel, respectively.

There are three momentum conservation (x, y, z directions) [97]:

$$\nabla.\mu\nabla\mathrm{v}_x - \nabla.(\rho V v_x) - \frac{\partial P}{\partial x} = \rho\frac{\partial v_x}{\partial t}, \tag{5}$$

$$\nabla.\mu\nabla\mathrm{v}_y - \nabla.(\rho V v_y) - \frac{\partial P}{\partial y} = \rho\frac{\partial v_y}{\partial t}, \tag{6}$$

$$\nabla.\mu\nabla\mathrm{v}_z - \nabla.(\rho V v_z) - \frac{\partial P}{\partial z} + \rho\gamma g(T - T_0) = \rho\frac{\partial v_z}{\partial t}, \tag{7}$$

where, μ, P, v_x, v_y, v_z are represents the effective viscosity, the pressure and the velocity mechanisms in the x, y, and z direction, respectively. The period $\rho\gamma g(T - T_0)$ represents resilience forces in terms of the Boussinesq approximation.

In EAF, there is a Turbulence model that the standard $k - \varepsilon$ turbulence model is used in this paper [97].

$$\frac{\partial(\rho k)}{\partial t} + \nabla.(\rho kV) = \nabla.\left(\frac{\mu}{\sigma_k}\nabla\mathrm{k}\right) + G - \rho\varepsilon, \tag{8}$$

conservation of the dissipation rate of turbulent kinetic energy, ε, is expressed as followed [97]:

$$\frac{\partial(\rho\varepsilon)}{\partial t} + \nabla.(\rho\varepsilon V) = \nabla.\left(\frac{\mu}{\sigma_\varepsilon}\nabla\varepsilon\right) + \frac{G}{k}(C_1G - C_1\rho\varepsilon), \tag{9}$$

where, C_1, C_1, σ_ε *and* σ_k are 1.44, 1.92, 1.0, and 1.3, respectively.

The boundary conditions for bottom were as following:

$$\begin{aligned} &v_x = v_y = 0 \quad \textit{for non slip condition} \\ &v_z = 0 \quad \textit{for impermeabiliy} \end{aligned} \tag{10}$$

Turbulence limits (k and ε) are zero at the ramparts then near to the walls the flow regime has to remain laminar. For side wall that alike to the bottom wall zero velocities are allotted at this wall because of the non-slip condition and waterproofness of the receptacle, and turbulence for these walls are zero.

$$\begin{aligned} &v_x = v_y = 0 \quad \textit{for non slip condition} \\ &v_z = 0 \quad \textit{for impermeabiliy} \end{aligned} \tag{11}$$

Heat flow from the melt to the environs finished the lateral furnace walls of part was calculated alike to the bottom wall as showed underneath [97]:

$$Q = -k_{MgO} * A\frac{\partial(T)}{\partial x} - k_{MgO} * A\frac{\partial(T)}{\partial y}, \tag{12}$$

for allowed surface, subsequently no slag is painstaking in the EAF, the gas atmosphere overhead the melt prepares not fleece the liquid steel. Formerly, shear (τ_{zy} and τ_{zx}) from the gas stage to the liquid bath is set to be zero, as designated underneath:

Zero shear at the free surface in the y-direction [97]:

$$\tau_{zy} = -\mu\frac{\partial(v_y)}{\partial z}, \tag{13}$$

$$\tau_{zx} = -\mu\frac{\partial(v_x)}{\partial z}, \tag{14}$$

and liquid steel does not flow out at the free surface:

$$v_z = 0, \tag{15}$$

and, zero gradients of turbulence at the free surface:

$$\frac{\partial k}{\partial z} = \frac{\partial \varepsilon}{\partial z} = 0, \tag{16}$$

from the free surface of the melt with an area (A) to the surroundings at a temperature (T_s)j, there is a radiation exchange (Q_{rad}):

$$Q_{rad} = -\sigma\dot{\varepsilon}A\left(T^4 - T_s^4\right), \tag{17}$$

where, σ is the Stefan-Boltzmann's constant $\left(5.67 * 10^{-8}\frac{W}{m^2 * K^4}\right)$ and $\dot{\varepsilon}$ is the emissivity of the liquid steel (0.8). The three zones connected to the electric arcs release heat through radiation like the remaining exposed surface. However, these zones also receive a substantial heat influx from the electric arcs. When considering a specific combination of electric parameters, such as voltage and arc length, the power input (P_0) signifies the amount of heat supplied, as outlined below:

$$P_0 = -k\frac{\partial T}{\partial z}, \tag{18}$$

and all physical properties of molten steel were applied in Table 1 [97].

Fig. 8 illustrates temperature profiles at the liquid steel's exposed surface from an overhead perspective, showcasing distinct arc lengths. This view highlights the extent of the highly heated region relative to the arc length. An essential aspect pertains to the injection point of DRI particles, positioned between phases 2 and 3, ideally near the pitch circle. Operating the furnace with a longer arc length ensures that DRI particle melting rates increase within the superheated zone, leading to the following results achieved under standard conditions defined by a 45 cm arc length and an extreme arc voltage of 1210 V.

Consequence of frothy slag height on hot spots formation inside the electric arc furnace according to a radiation model was studied by Sanchez et al. [98]. An industrial-scale model has been developed to predict the formation of hot spots in a large EAF with extended arc operation (45 cm) and a maximum tap voltage of 1210 V. This model takes into account the effect of frothy slag height on hot spot formation in the EAF. They used the FLUENT version 6.2.16 software to advance the radiation model. Thermal conductivities and emissivity employed for electrode (with Graphite), water cooled panels (with steel) and slag refractory (with MgO) are 230, 75.85 and 4 W/m.K and 0.85, 0.8 and 0.31, respectively. In Fig. 9, you can observe the three plasma regions, with the shaded rectangular area representing the slag door. The electrode situated closest to the slag door is referred to as phase 1. The energy in this phase can be entirely lost if the plasma is left uncovered. Conversely, it can be fully harnessed to heat the underlying liquid phases beneath the three plasmas when the slag height is maintained at 45 cm. To quantify this, they established a measure of energy radiated relative to slag height, as detailed in Table 2. Their findings indicate that enhancing the thermal efficiency of the electric arc furnace is achievable by reducing the intensity of incident radiation through the use of a frothy slag that covers a minimum of 75 % of the arcs, which is equal to 2.07 MW/m^2 of incident radiation. Taking into consideration the conditions to prevent the formation of hot spots during EAF operation, it becomes possible to recover and utilize up to 25 % of the total energy supplied by the power system for the purpose of metal melting (see Fig. 10 [98]).

Gruber et al. [99] conducted a mathematical modeling study to examine the impact of the arc area on heat and mass transfer in an EAF. The EAF model had specific geometric dimensions, as depicted in the provided Fig. 11 and Table 3. For this research, the higher vessel walls of the EAF were equipped with chilling panels as boundary conditions. In contrast, the lower vessel's walls were primarily composed of fire bricks and other refractory materials. Together the upper and lower vessel interiors in the freeboard were typically covered with a slag layer. In this investigation, the thermal conductivity of both the dust and slag layer was assumed to be 2.2 W/m.K,

Table 1
Physical properties of molten steel [97].

Parameters	Value	Unit
Density	$7.2 * 10^3$	$\frac{Kg}{m^3}$
Specific heat at constant pressure	670	$\frac{J}{kg.K}$
Viscosity	$6.5 * 10^{-3}$	$\frac{Kg}{m.s}$
Thermal Conductivity	15	$\frac{W}{m.K}$
Emissivity of bath surface	0.8	
Thermal coefficient of volume expansion	$1.4 * 10^{-3}$	$\frac{1}{K}$

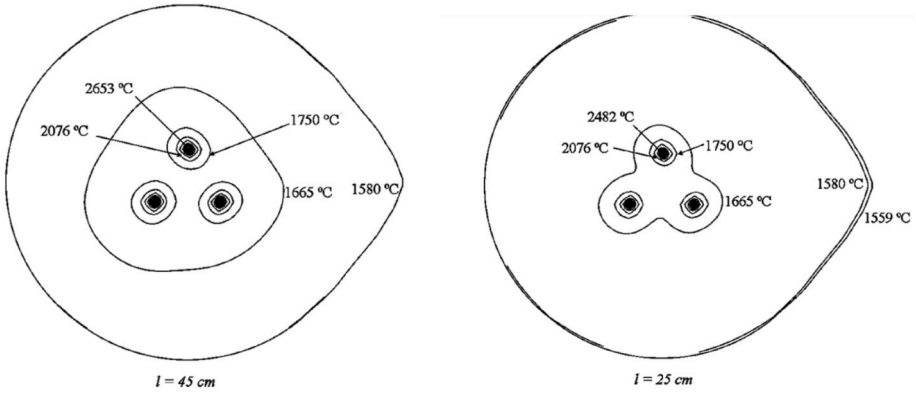

Fig. 8. Temperature fields as a function of arc length, Top view [97].

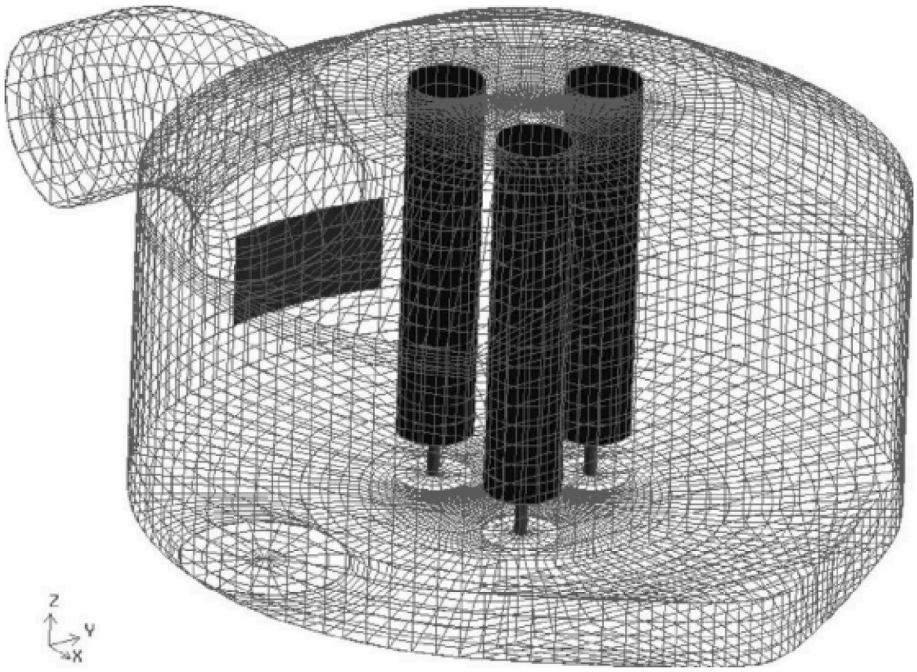

Fig. 9. Computational domain of the industrial EAF, including electrodes and arc [98].

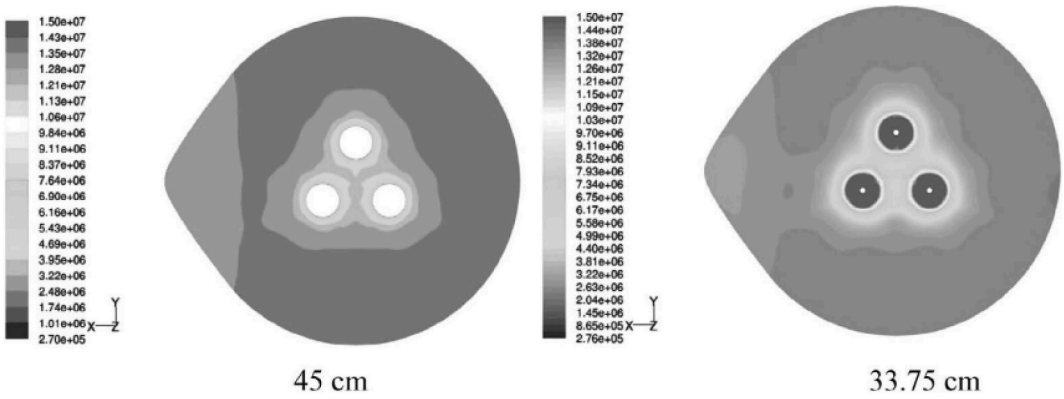

Fig. 10. Incident radiation in W/m2 on the slag surface as a function of slag height [98].

Table 2
Radiation intensity as a function of slag height

Slag height (cm)	Arc Covered (%)	Exposed Surface (m^2/arc)	Radiation (MW/arc)	Total radiation (MW)
0	0	0.1685	10.11	30.33
11.25	25	0.1263	7.58	22.74
22.5	50	0.0842	5.05	15.15
33.75	75	0.0421	2.52	7.56
45	100	0	0	0

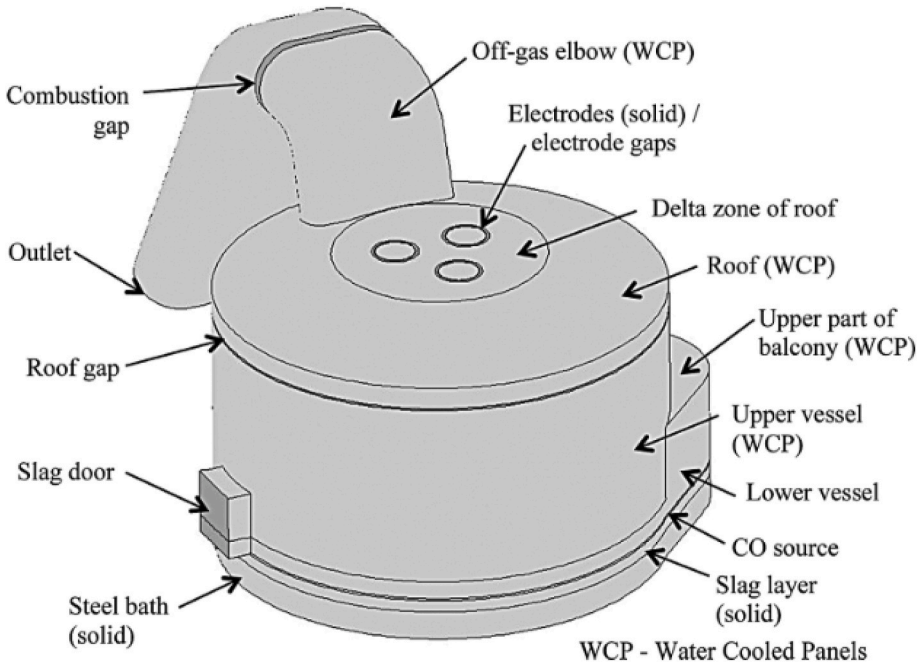

Fig. 11. EAF CFD model [99].

Table 3
Parameters of EAF model

Parameters	Value
diameter of the electric arc furnace vessel	6.100 m
Height of vessel	3.824 m
slag door's height	0.650 m
slag door's width	0.900 m
fourth hole's surface	2.090m^2
Size of electrode gaps	0.040 m
Size of roof gap	0.030 m
steel bath layer's height	0.400 m
Vertical distance from top of steel bath to bottom of slag door	0.200 m
Height of slag layer (solid)	0.170 m
Height of slag CO source layer	0.030 m
Electrode's diameter	0.559 m
Length of electric arc	0.400 m
Radius of electric arc	0.045 m
Arc region: length of negative velocity inlet and mass flow inlet	0.050 m

with a slag layer height of 170 mm. To simulate the inflow into each arc, a negative velocity inlet was defined at the top of the arc column, where fluid was drawn out of the domain at a velocity of 338 m/s, corresponding to a mass flow rate of 0.44 kg/s as determined by the arc model. This inlet velocity was deemed acceptable in comparison to radial velocities of around 400 m/s observed in prior research. In proximity to each arc's foundation, a related mass-flow inlet was defined, through which 0.44 kg/s of CO at a temperature of 5500 K entered the system. It was presumed that the outflow temperature from the arcs coincided with the time-averaged thermal radiation temperature of the AC arc channels. To account for the high carbon monoxide concentration around

the base of the electrodes resulting from the CO source well-defined at the slag surface, the mass fraction of CO was set to 1 at the mass flow cove. As can be seen in Fig. 12, The highest temperature observed in the simulation for the water-cooled upper vessel reached 2139 K. At this temperature, it is anticipated that the protective slag layer covering the vessel's water-cooled panels would melt, potentially causing damage to the panels. Typically, to prevent panel perforation, the maximum allowable temperature is around 1800 K. It's worth noting that this simulation considers a slag height of approximately 43 % of the arc length, and as a result, the arcs are replicated as comparatively unrestricted red-hot arcs. While this outcome may not be ideal in actual EAF operations, it remains a realistic representation of the conditions.

The primary findings from this study, as inferred from the presented results, can be summarized as follows.

- The influence of inflow and outflow in the arc region is a significant factor that should not be disregarded, as it constitutes a notable energy input mechanism for the arc region. This effect enhances socializing and promotes post-combustion of gas species within the furnace.
- When analyzing energy flows in the current EAF model, it develops apparent that the inclusion of graphite electrodes is imperative to accurately model the redeployment of energy within the furnace.
- To ultimately achieve the long-term objective of comparing real electric energy input with modeled energy flows, it is crucial to delve deeper into the investigation of separate energy sources and basins within the arc region and the molten soak.

As can be seen in Fig. 13, the corporeal and chemical possessions of melted bath with bottom-blowing in EAF processes was studied by Wei et al. [100]. This study provides valuable insights on the possessions of bottom-blowing gas flow degree on the fluid flow appearances in the EAF melted bath. It also highlights the advantages of bottom-blowing technology in indorsing heat transfer and metallurgical reactions in the molten bath. Bottom-blowing technology is a widely adopted technique in EAF steelmaking process. It involves injecting gas from the bottom of the furnace to promote the fluid flow of the molten bath, accelerate the metallurgical response, and enhance the quality of melted steel. Raising the bottom-blowing gas flow rate has several beneficial effects. It reduces the mixing time of the liquid bath, increases the typical fluid flow velocity in the molten bath, and reductions the dead zone volume. Additionally, this technology enhances bath stirring, leading to improved temperature uniformity, higher heat transfer rates, and faster overall heating of the molten bath. It also accelerates the melting of steel scrap and alloys. When compared to traditional melting conditions without bottom-blowing, it results in a reduction of phosphorus content in the molten steel by 0.005 mass percent, as well as decreased levels of FeO and T. Consequently, bottom-blowing technology significantly enhances the excellence of molten steel produced in the EAF steelmaking process by improving product quality and reducing impurities. In summary, increasing the bottom-blowing gas flow rate in the EAF molten bath speeds up fluid flow and reduces the dead zone volume. The liquid bath's mixing time reduces, and the average fluid flow velocity in the molten bath increase. The results of numerical simulations clearly show that the impact of the bottom-blowing gas flow rate on the fluid dynamics in the electric bottom blowing area is especially pronounced. The communication amongst the bottom-blowing gas brooks effects the melted bath flow field 1. Therefore, cumulative the

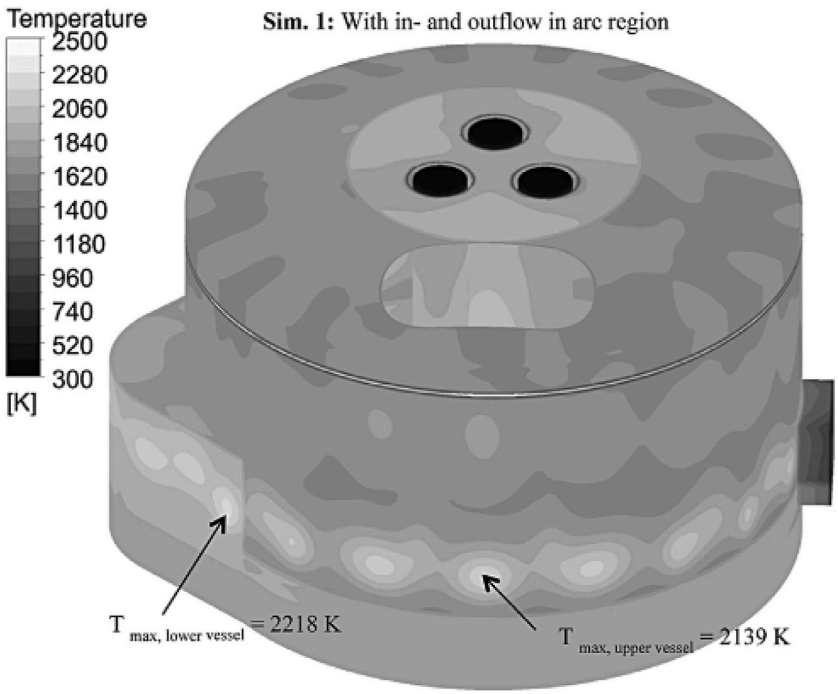

Fig. 12. Temperature distribution on the EAF walls for simulations [95].

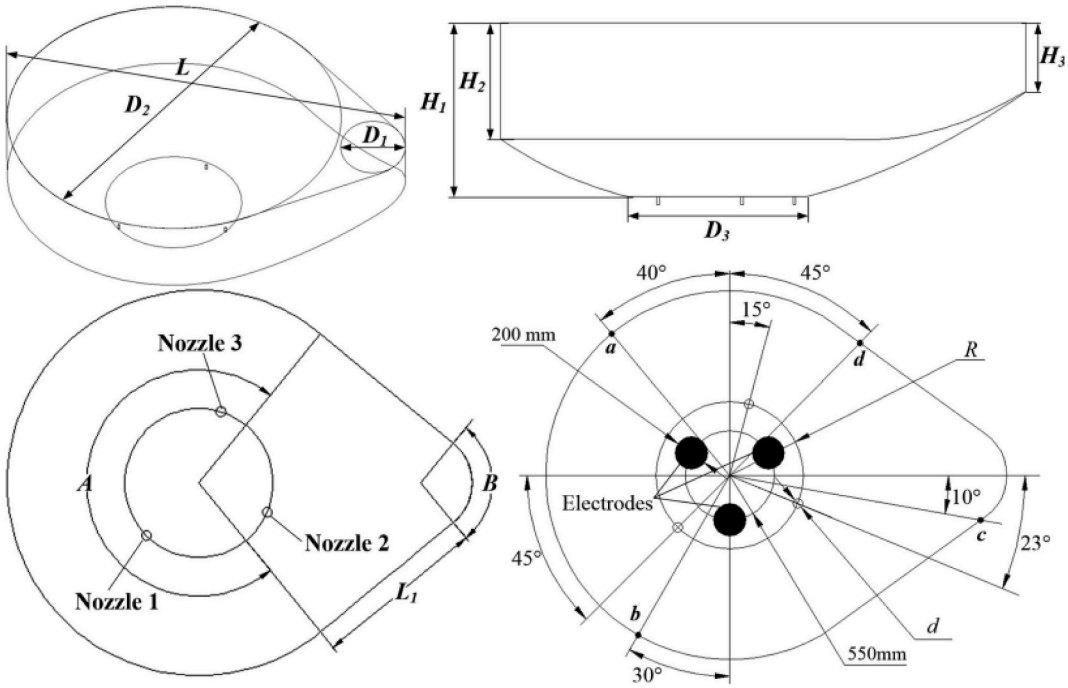

Fig. 13. Geometry of EAF [100].

bottom-blowing gas flow rate container improve the fluid flow characteristics in the EAF molten bath. Geometry parameters was written in Table 4.

Fig. 14 illustrates the delivery of fluid flow velocities within the melted bath along a longitudinal section, highlighting various gas flow rates used for bottom blowing. Different colors in Fig. 14 denote distinct fluid flow velocities, with red and blue indicating the maximum and minimum velocities, respectively. The depiction in Fig. 14 reveals the presence of three areas with low flow speeds denoted as Region A, Region B, and Region C within the molten bath. Region A corresponds to the zone near electric bottom blowing area, Region B is situated in proximity to the electric arc furnace opening, and Region C is positioned amidst the three bottom-blowing nozzles. Evidently, as the rates of bottom-blowing gas flow increase, the low flow velocity areas (Region A, B, and C in Fig. 14) diminish, leading to a gradual rise in the molten bath's flow velocity. The impact of the bottom-blowing gas flow rate is particularly pronounced in the EBT area. At a gas flow rate of 50 L/min, the flow velocity in the EBT area ranges from 0.0001 to 0.002 m/s, while at a flow rate of 200 L/min, it exceeds 0.02 m/s. This indicates a substantial increase in flow velocity with higher gas flow rates.

Fig. 15a displays the instantaneous velocity circulation throughout the entire furnace. Notably, the pressure is excessively high, resulting in furnace gas escaping complete the slag door. The oxygen jets stand visually represented as blue iso-surfaces and displace the lighter slag (red) as they enter into the melt (yellow) at varying depths. It is observed that these oxygen jets typically reach a

Table 4
geometric parameters in Ref. [100].

Items	EAF Prototype
EAF capacity	75 ton
D1	1249 mm
D2	3700 mm
D3	1928 mm
H1	1700 mm
H2	1252 mm
H3	600 mm
L	5774 mm
L1	2444 mm
A	110 (o)
B	233 (o)
R	909 mm
D	4980 Dp
d	10 dp
H	1300
Molten steel depth	150
Slag layer thickness	1450H9

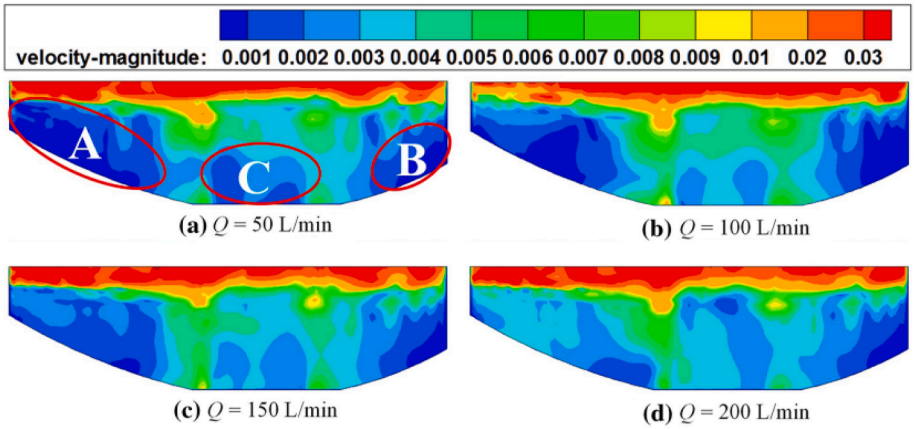

Fig. 14. Velocity distribution in the molten bath on longitudinal section.

penetration depth of approximately 0.1–0.2 m, which aligns with the findings of Koria and Lange [101]. The injection of oxygen jets induces mild agitation in the melt bath and on the melt's surface, as illustrated in Fig. 15b. Importantly, this injection does not lead to splashing of the melt against the electrodes. The positioning of the injectors is such that the oxygen jets are directed between the electrodes, preventing high velocities beneath the injector box. The slag layer is penetrated by these oxygen jets, causing partial displacement of the arcs. Consequently, the arcs temporarily emit heat towards the furnace wall, resulting in the generation of hot spots in the vicinity of the slag door, with temperatures reaching up to T_{max} (equals 1580 °C). This phenomenon may lead to refractory lining overheating and potential cooling panel issues [102]. In summary, Fig. 15a highlights issues related to high pressure at the off-gas elbow and the displacement of the slag layer by oxygen jets. These jets induce mild agitation in the melt without causing splashing against the electrodes, but their effect on arc behavior and temperature distribution can have consequences for refractory materials and cooling panels.

In the study directed by Rafiei et al. [103], they explored the impact of temperature on electrode consumption in a scenario where the electrode diameter (D) is 0.6 m and the electrode length is 7.2 m. They employed a steady-state ANSYS-Mechanical APDL simulation, utilizing a three-dimensional model comprising 1800 elements. The simulation revealed that at the tip of the electrode, the temperature reductions over a span of approximately 0.4 m, ranging from 3600 to 1500 K. The findings of the study indicate that there is a mutual influence among the electrodes regarding their surface temperatures. An important conclusion drawn from this research is that to accurately simulate the physical effects occurring within the arc, sub-models are necessary. Unless the intention is to solely simulate a limited area around the arc, computational-aided modeling offers a balanced approach, providing a good compromise between physical precision and computational efficiency. Furthermore, the Lorentz force was observed to direct the arc radially outward, as illustrated in Fig. 16, causing an extension of the arc length. The study revealed that 4 MW of energy are emitted in the form of radiation at a temperature of 15,000 K, with an arc power of 140 MW. It's worth noting that this power emission is relatively low compared to data reported by other researchers. The simulation was able to replicate the restrained standards of present and voltage from the field test, but solitary after the presence of iron (Fe) vapor was taken into account.

In a study conducted by Rafiei et al. [103], the impact of temperature on electrode ingesting was investigated. The simulation was based on a steady-state ANSYS-Mechanical APDL model in three dimensions, utilizing approximately 1800 elements. The simulation focused on an electrode with dimensions of D = 0.6 m and L = 7.2 m. At the tip of the electrode, a significant temperature decrease was observed over a length of approximately 0.4 m, ranging from 3600 K to 1500 K. The research findings revealed that the electrodes mutually influence one another in terms of their surface temperatures. It was concluded that accurately simulating the physical phenomena within the arc requires sub-models. While channel arc model simulations offer a reasonable compromise between physical accuracy and computational efficiency, it's important to note that they may not encompass the entire arc region unless the intention is to pretend a minor part about the arc exclusively. The Lorentz force plays a crucial role in steering the arc radially towards the outer regions, as depicted in Fig. 17. This effect leads to an elongation of the arc. In this process, approximately 4 MW of energy are produced as radiation at a temperature of T_{arc}, 15,000 K, and the arc's power amounts to $P_{arc} = 140$ MW. It's worth noting that this power level is relatively low when compared to data from other research studies. To accurately reproduce the unrushed standards of contemporary and voltage obtained from field tests, the simulation needed to take into account the presence of iron vapor. In summary, Rafiei et al.'s study explored the relationship between temperature and electrode consumption through sophisticated simulations, emphasizing the importance of sub-models and considering the Lorentz force's role in arc behavior, highlighting the significance of iron vapor for accurate simulations of current and voltage in electric arc furnaces.

6. Conclusion

Computational Fluid Dynamics (CFD) is a numerical modeling technique that plays a vital character in assumed and optimizing the operations of an EAF. In the context of an EAF, CFD is utilized to simulate and analyze the complex interactions of fluids, heat, and

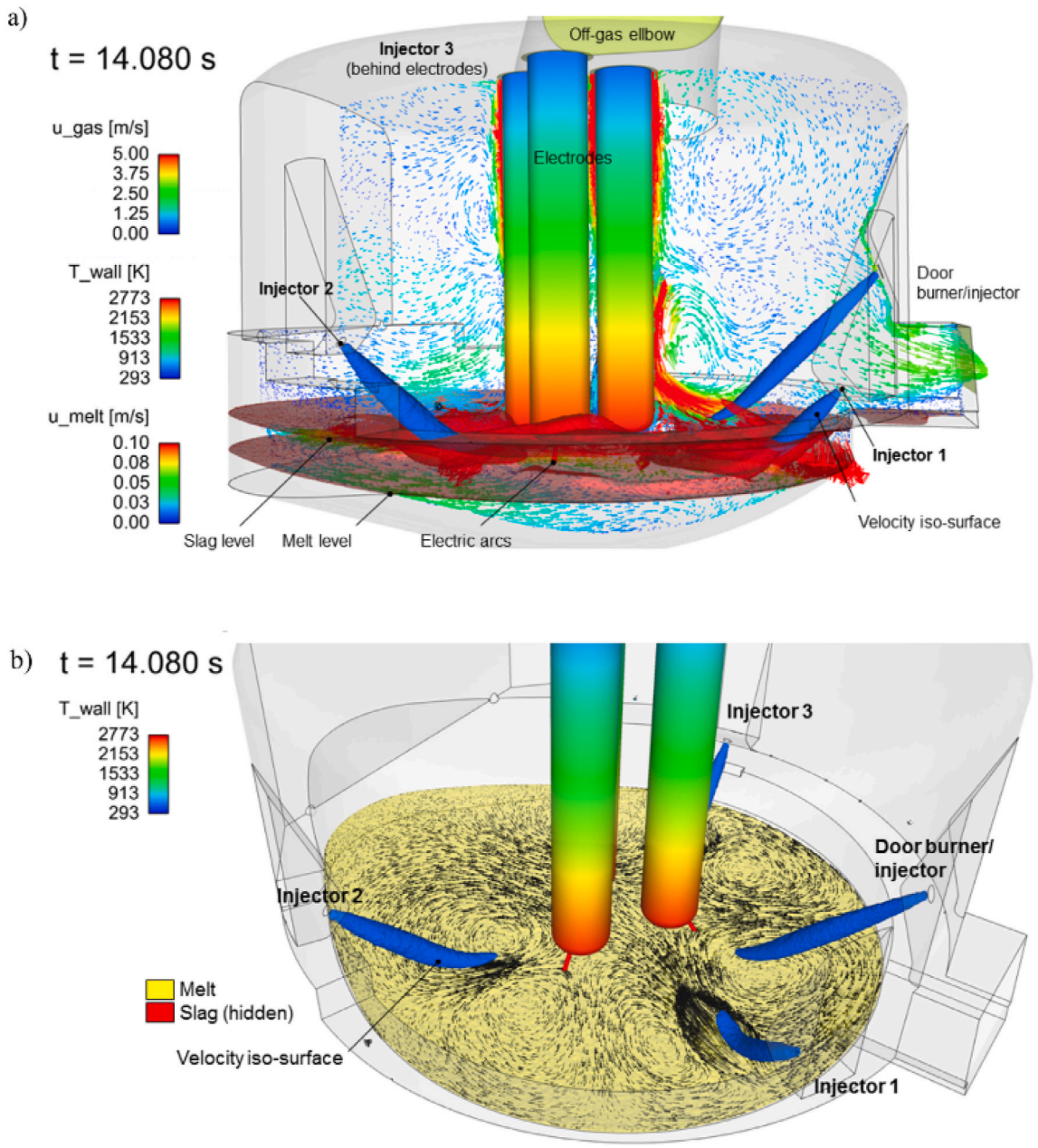

Fig. 15. CFS simulation of EAF [101,102].

materials within the furnace. CFD of fluid dynamics simulation, chemical reactions, energy balance, electrode and arc modeling, and optimization of EAF was studied in most researched. The novelty in this review of EAF lies in its ability to provide a consolidated and up-to-date overview of the research and advancements related to EAF steelmaking.

It is recommended that future research should consider the following areas of investigation.

- **DRI Dropping Point:** During a site visit to an Iranian steel factory, it was observed that sponge iron is stored overhead. A critical aspect that warrants simulation is the process by which sponge iron is introduced into the furnace.
- **Reduction of Small DRI:** An essential area for study involves the examination of various dimensions of small sponge iron and finding solutions to prevent its fragmentation prior to entering the furnace.
- **Electrode Arrangement Analysis:** The configuration of electrodes is a vital component within the electric arc furnace. Exploring different electrode arrangements and analyzing their impact on melting times within various magnetic fields is of great significance.

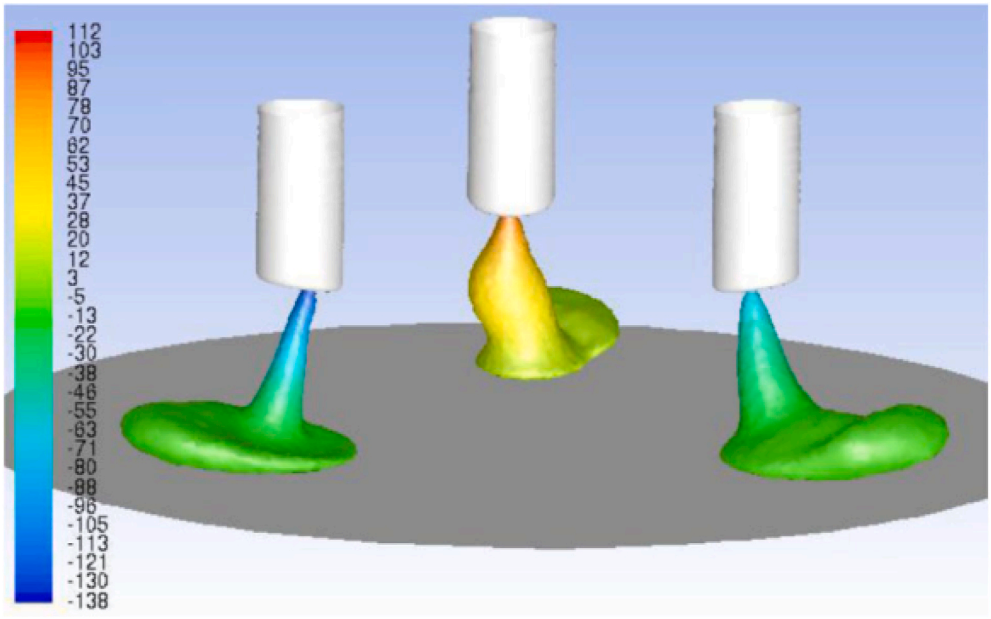

Fig. 16. An extension of the arc length in EAF [103].

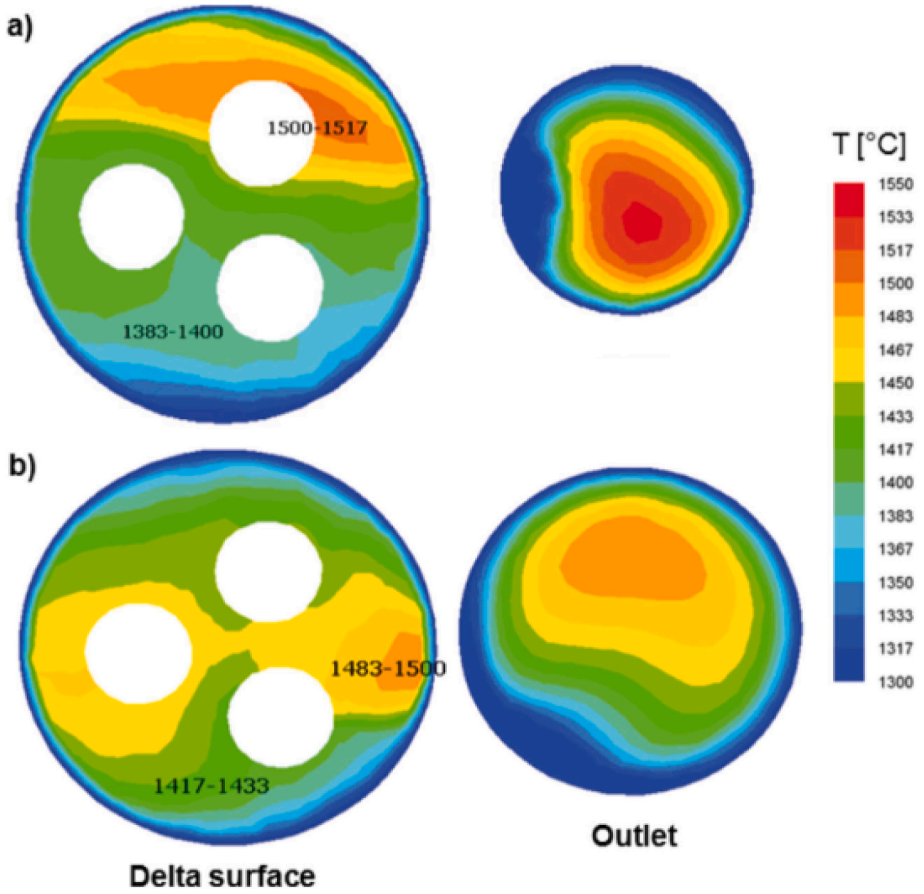

Fig. 17. Melting temperature in the EAF [104].

- **Proportion of Scrap Iron and DRI:** A key focus for future endeavors is to investigate the presence of scrap iron and understand its influence during the melting of sponge iron in the furnace. This research will shed light on the role and efficiency of both materials in the steelmaking process.
- **Modeling of Hot Charge of EAF:** In these future research areas, an in-depth exploration of sponge iron, its handling with hot charge, and interactions within the electric arc furnace is proposed. This investigation holds the potential to enhance the efficiency and performance of the steelmaking process.
- **Data-Driving Modeling**: leveraging data-driving approaches, such as machine learning and statistical modeling, to extract insight from large datasets and improve the predictive accuracy of EAF models.
- **Modeling of DRI-EAF based on Green Steel:** Given the current global inclination towards green steel initiative, the utilization of green hydrogen to rejuvenate steel production becomes crucial. Within the DRI-EAF technology, there is greater prevalence of hydrogen steel projects compared to the BF-BOF technology. So, it underscores the significance of modeling and simulating technology DRI-EAF based on renewable energy.
- **Sustainability Analysis:** incorporating sustainability metrics, such as energy efficiency, energy intensity, greenhouse gas emissions, and resource utilization, into EAF models to evaluate the environmental performance of different process configurations and operational strategies.

By addressing these research areas and implementing improvements, modeling efforts for EAFs can advance significantly, leading to more accurate, reliable, and insightful tools for process optimization and design in the steel industry.

CRediT authorship contribution statement

Mahmoud Makki Abadi: Validation, Methodology, Conceptualization. **Hongyan Tang:** Visualization, Project administration, Formal analysis. **Mohammad Mehdi Rashidi:** Supervision, Resources, Formal analysis, Conceptualization.

Declaration of competing interest

There is no conflict of interests between the authors.

References

[1] P. Mhatre, V.V. Gedam, S. Unnikrishnan, Material circularity potential for construction materials–The case of transportation infrastructure in India, Resour. Pol. 74 (2021) 102446.
[2] L.G. Carmona, K. Whiting, H. Haberl, T. Sousa, The use of steel in the United Kingdom's transport sector: a stock–flow–service nexus case study, J. Ind. Ecol. 25 (1) (2021) 125–143.
[3] M.H. Joulazadeh, A. Etemad, Evaluation of the production of DRI in the world and Iran in 2021, International Journal of Iron & Steel Society of Iran 19 (1) (2022) 55–66.
[4] M. Ramezani Moziraji, G.A. Dezvareh, M. Ehteshami, M.R. Sabour, A. Bazargan, Life cycle assessment of gas-based EAF steel production: environmental impacts and strategies for footprint reduction, Int. J. Life Cycle Assess. 28 (12) (2023) 1605–1621.
[5] S.K. Dutta, Y.B. Chokshi, S.K. Dutta, Y.B. Chokshi, Electric Furnace Processes, Basic Concepts of Iron and Steel Making, 2020, pp. 401–496.
[6] M. Chaabet, E. Dötsch, Steelmaking based on inductive melting, Induction Technology (1) (2012) 49–58.
[7] V. Turkovskyi, A. Malinovskyi, A. Muzychak, V. Lysiak, The characteristics study of the pilot power supply of a smallcapacity electric arc furnace with a non-valve converter" constant current-constant voltage", Przeglad Elektrotechniczny 99 (6) (2023).
[8] M. Kaya, Galvanizing residue and electrical Arc Furnace (EAF) dust, in: Recycling Technologies for Secondary Zn-Pb Resources, Springer International Publishing, Cham, 2023, pp. 71–150.
[9] Z. Yan, S. Yang, W. Liu, J. Li, Simulation study on the influence of thickness and relative foaming height of refining slag on electrothermal characteristics in ladle furnace, J. Mater. Res. Technol. 27 (2023) 75–91.
[10] K. Karalis, N. Karalis, N. Karkalos, N. Ntallis, G.S.E. Antipas, A. Xenidis, Three-dimensional computational fluid dynamics analysis of an electric submerged arc furnace, Sci. Rep. 11 (1) (2021) 17637.
[11] K. Solonchenko, O. Rybalkina, D. Chuprynina, E. Kirichenko, K. Kirichenko, V. Nikonenko, Stability of properties of layer-by-layer coated membranes under passage of electric current, Polymers 14 (23) (2022) 5172.
[12] A. Treppschuh, K. Krueger, R. Kuehn, H. Schliephake, Thermal based power control of a DC-EAF, Arch. Metall. Mater. 53 (2) (2008) 425–430.
[13] K. Bergman, B. Kjellberg, N. Ringvägen, DC arc furnace technology applied to smelting applications, in: Proceedings of the Ninth International Ferroalloys Congress, Quebec City, Canada, 2001, June, pp. 80–89.
[14] T. Wieczorek, K. Mączka, Modelling of the AC-EAF process using computational intelligence methods, Przeglad Elektrotechniczny 84 (11) (2008) 184–188.
[15] E. Durna, C.Ö. Gerçek, Ö. Salor, M. Ermiş, Suppression of the second harmonic subgroup injected by an AC EAF: design considerations and performance estimation of a shunt APF, Electronics 7 (4) (2018) 53.
[16] H. Akeiber, P. Nejat, M.Z.A. Majid, M.A. Wahid, F. Jomehzadeh, I.Z. Famileh, S.A. Zaki, A review on phase change material (PCM) for sustainable passive cooling in building envelopes, Renew. Sustain. Energy Rev. 60 (2016) 1470–1497.
[17] N. Choab, A. Allouhi, A. El Maakoul, T. Kousksou, S. Saadeddine, A. Jamil, Review on greenhouse microclimate and application: design parameters, thermal modeling and simulation, climate controlling technologies, Sol. Energy 191 (2019) 109–137.
[18] G.A.O. Rocha, M.A. Pichimata, E. Villagran, Research on the microclimate of protected agriculture structures using numerical simulation tools: a technical and bibliometric analysis as a contribution to the sustainability of under-cover cropping in tropical and subtropical countries, Sustainability 13 (18) (2021) 10433.
[19] P.C.J. Hoi, *Validation Of Discrete Ordinate Radiation Model for Application in UV Air Disinfection Modeling* (Doctoral Dissertation), 2014.
[20] L. Wang, J. Chen, C. Wu, Auxiliary energy-assisted arc welding processes and their modelling, sensing and control, Sci. Technol. Weld. Join. 26 (5) (2021) 389–411.
[21] M. Tunc, U. Camdali, G. Arasil, Mass analysis of an electric arc furnace (EAF) at a steel company in Turkey, Metallurgist 56 (2012) 253–261.
[22] T. Meier, V. Logar, T. Echterhof, I. Škrjanc, H. Pfeifer, Modelling and simulation of the melting process in electric arc furnaces—influence of numerical solution methods, Steel Res. Int. 87 (5) (2016) 581–588.
[23] F. Opitz, P. Treffinger, J. Wöllenstein, Modeling of radiative heat transfer in an electric arc furnace, Metall. Mater. Trans. B 48 (2017) 3301–3315.

[24] T. Meier, A.H. Kolagar, T. Echterhof, H. Pfeifer, Process Modeling and Simulation of an Electric Arc Furnace for Comprehensive Calculation of Energy and Mass Transfers in Combination with a Model of the Dedusting System, EEC, 2016.
[25] F. Illahi, I. El-Amin, M.U. Mukhtiar, The application of multiobjective optimization technique to the estimation of electric arc furnace parameters, IEEE Trans. Power Deliv. 33 (4) (2017) 1727–1734.
[26] F. Illahi, *Analysis And Mitigation of Effects of Electric Arc Furnace Operation on Shaft of Synchronous Generator* (Doctoral Dissertation, King Fahd University of Petroleum and Minerals (Saudi Arabia)), 2014.
[27] Y. Djeghader, H. Labar, K. Bounaya, Analysis of harmonics generated by different structures of a DC EAF. International Review on Modelling and Simulations, 2008, pp. 173–177.
[28] K. Bergman, R. Gonzales, M.A. Pedroza, M. Herrera, Twin cathode DC EAF concepts and results at Hylsa Mexico, Metallurgical Research & Technology 98 (1) (2001) 55–62.
[29] A. Murthy, J. Szekely, N. El-Kaddah, Experimental measurement and numerical computation of velocity and turbulence parameters in a heated liquid metal system, Metall. Trans. A B 19 (1988) 765–775.
[30] M. Al-Nasser, H. Barati, C. Redl, A. Ishmurzin, N. Voller, G. Hackl, A. Kharicha, Effect of compressibility on industrial DC electric arcs, Results in Engineering 19 (2023) 101312.
[31] P. Lv, X. Zhang, L. Chen, S. Wang, Z. Wang, R. He, L. Guan, Simulation and optimization of the auxiliary cathode for inter-electrode discharge electric field in microarc oxidation, Materials 16 (14) (2023) 5065.
[32] D. Kışla, G.G. Gökmen, G.A. Evrendilek, T. Akan, T. Vlčko, P. Kulawik, F. Ozogul, Recent developments in antimicrobial surface coatings: Various deposition techniques with nanosized particles, their application and environmental concerns, Trends Food Sci. Technol. 135 (2023) 144–172.
[33] X.Y. Gao, Mathematical view with observational/experimental consideration on certain (2+ 1)-dimensional waves in the cosmic/laboratory dusty plasmas, Appl. Math. Lett. 91 (2019) 165–172.
[34] R. Clough, A. Fisher, B. Gibson, B. Russell, Atomic spectrometry update: review of advances in the analysis of metals, chemicals and materials, J. Anal. Atom. Spectrom. 38 (2023) 2215–2279.
[35] M.A.V. Shinde, A. Vijayalakshmi, J. Pandit, M. Meena, Basics of Engineering Chemistry, AG PUBLISHING HOUSE, 2023 (AGPH Books).
[36] M. Skaf, J.M. Manso, Á. Aragón, J.A. Fuente-Alonso, V. Ortega-López, EAF slag in asphalt mixes: a brief review of its possible re-use, Resour. Conserv. Recycl. 120 (2017) 176–185.
[37] European Electric Steelmaking Conference, *7th European electric steelmaking conference*. Associazione Italiana di Metallurgia, 2002.
[38] V. Logar, D. Dovžan, I. Škrjanc, Modeling and validation of an electric arc furnace: Part 2, thermo-chemistry, ISIJ Int. 52 (3) (2012) 413–423.
[39] E. Khodabandeh, M. Ghaderi, A. Afzalabadi, A. Rouboa, A. Salarifard, Parametric study of heat transfer in an electric arc furnace and cooling system, Appl. Therm. Eng. 123 (2017) 1190–1200.
[40] Q. Reynolds, Thermal radiation modelling of DC smelting furnace freeboards, Miner. Eng. 15 (11) (2002) 993–1000.
[41] Y. Li, R.J. Fruehan, Computational fluid-dynamics simulation of postcombustion in the electric-arc furnace, Metall. Mater. Trans. B 34 (2003) 333–343.
[42] K.U. Vinayaka, P.S. Puttaswamy, Review on characteristic modeling of electric arc furnace and its effects, in: 2017 International Conference on Intelligent Computing, Instrumentation and Control Technologies (ICICICT), IEEE, 2017, July, pp. 1222–1229.
[43] S. Daneshmand, M.H. Vini, Investigation of TiO2/SiC coating on graphite electrodes for electrical Arc Furnaces, J. Mater. Eng. Perform. (2023) 1–19.
[44] I. Makrygiannis, K. Karalis, Optimizing building thermal insulation: the impact of brick Geometry and thermal coefficient on energy efficiency and comfort, Ceramics 6 (3) (2023) 1449–1466.
[45] X.K. Zhang, Y.L. He, S.Z. Tang, F.L. Wang, T. Xie, An electromagnetics-temperature-component multi-physical coupled model for electric furnace in calcium carbide smelting process, Appl. Therm. Eng. 165 (2020) 114552.
[46] H.N. Cui, T. Li, C.G. Bai, M. Tan, Y.L. Zhu, Numerical simulation of coupling multi-physical field in electrical arc furnace for smelting titanium slag, J. Iron Steel Res. Int. (2023) 1–16.
[47] Y. Saboohi, A. Fathi, I. Škrjanc, V. Logar, Optimization of the electric arc furnace process, IEEE Trans. Ind. Electron. 66 (10) (2018) 8030–8039.
[48] S. Shyamal, C.L. Swartz, Optimization-based online decision support tool for electric arc furnace operation, IFAC-PapersOnLine 50 (1) (2017) 10784–10789.
[49] S. Matson, W.F. Ramirez, Optimal operation of an electric arc furnace, in: 57 Th Electric Furnace Conference, 1999, pp. 719–730.
[50] M. Modigell, A. Traebert, P. Monheim, A modeling technique for metallurgical processes and its applications, AISE Steel Technol. 78 (2) (2001) 45–47.
[51] P. Nyssen, R. Colin, S. Knoops, Application of a dynamic metallurgical model to the electric arc furnace, Rev. Métall. 101 (4) (2004) 317–326.
[52] D. Guo, G.A. Irons, Modeling of radiation intensity in an EAF, in: Third International Conference of CRD in the Minerals and Process Industry, 2003, December, pp. 223–228.
[53] G. Andonovski, S. Tomažič, Comparison of data-based models for prediction and optimization of energy consumption in electric arc furnace (EAF), IFAC-PapersOnLine 55 (20) (2022) 373–378.
[54] S. Tomažič, G. Andonovski, I. Škrjanc, V. Logar, Data-driven modelling and optimization of energy consumption in EAF, Metals 12 (5) (2022) 816.
[55] V. Manojlović, Ž. Kamberović, M. Korać, M. Dotlić, Machine learning analysis of electric arc furnace process for the evaluation of energy efficiency parameters, Appl. Energy 307 (2022) 118209.
[56] J.D. Hernández, L. Onofri, S. Engell, Modeling and energy efficiency analysis of the steelmaking process in an electric arc furnace, Metall. Mater. Trans. B 53 (6) (2022) 3413–3441.
[57] T. Hay, V.V. Visuri, M. Aula, T. Echterhof, A review of mathematical process models for the electric arc furnace process, Steel Res. Int. 92 (3) (2021) 2000395.
[58] B. Tian, G. Wei, H. Hu, R. Zhu, H. Bai, Z. Wang, L. Yang, Effects of fuel injection and energy efficiency on the production and environmental parameters of electric arc furnace-heat recovery systems, J. Clean. Prod. 405 (2023) 136909.
[59] S. Zhang, D. Jiang, Z. Wang, F. Wang, J. Zhang, Y. Zong, S. Zeng, Predictive modeling of the hot metal sulfur content in a blast furnace based on machine learning, Metals 13 (2) (2023) 288.
[60] M.M. Rashid, P. Mhaskar, C.L. Swartz, Multi-rate modeling and economic model predictive control of the electric arc furnace, J. Process Control 40 (2016) 50–61.
[61] M. Kirschen, K. Badr, H. Pfeifer, Influence of direct reduced iron on the energy balance of the electric arc furnace in steel industry, Energy 36 (10) (2011) 6146–6155.
[62] V. Logar, I. Škrjanc, Modeling and validation of the radiative heat transfer in an electric arc furnace, ISIJ Int. 52 (7) (2012) 1225–1232.
[63] M. Klimas, D. Grabowski, Identification of nonstationary parameters of electric arc furnace model using Monte Carlo approach, in: 2020 Progress in Applied Electrical Engineering (PAEE), IEEE, 2020, June, pp. 1–6.
[64] E. Ruiz, D. Ferreño, M. Cuartas, L. Lloret, P.M. Ruiz del Árbol, A. López, F. Gutiérrez-Solana, Machine learning methods for the prediction of the inclusion content of clean steel fabricated by electric arc furnace and rolling, Metals 11 (6) (2021) 914.
[65] S.W. Choi, B.G. Seo, E.B. Lee, Machine learning-based tap temperature prediction and control for optimized power consumption in stainless Electric Arc Furnaces (EAF) of steel plants, Sustainability 15 (8) (2023) 6393.
[66] https://worldsteel.org/.
[67] X. Xi, S. Li, C. Li, H. Pan, J. Wang, R. Zhu, Research on technical parameters of electrical arc furnace steelmaking based on direct reduced iron as raw material, Ironmak. Steelmak. (2024) 03019233241238060.
[68] X. Wang, C. Deng, G. Xing, J. Ding, Q. Zhu, Z. Wang, C. Yu, High temperature mechanical properties of novel MgO–Al3BC3 refractories for electric arc furnace lining, Construct. Build. Mater. 426 (2024) 136219.
[69] https://www.vepica.com/blog/steel-production-from-iron-ore-to-functional-industrial-products.
[70] S. Huang, X. Long, Y. Cui, L. Zhang, Study on mechanism of titanium slag smelting in DC electric Arc Furnace, J. Phys. Conf. 2459 (1) (2023, March) 012053. IOP Publishing.

[71] S. Pavlovs, A. Jakovics, A. Chudnovsky, Melt azimuthal rotation in direct current electric arc furnace without external axial magnetic field, Int. J. Appl. Electromagn. Mech. (Preprint) (2024) 1–13.
[72] A.E. Fadel, A.L. Khalil, A.H. El-Nawagy, A.M. Futooh, M.A. Amer, Design of Industrial Furnace (End Port Glass Type) Prepared by, 2023.
[73] M.S. Moholwa, S.P. Tsebe, D.A. Hayman, P.J.A. Bezuidenhout, M.B. Sitefane, J.D. Steenkamp, Effect of ore pre-heating on furnace operation in high carbon ferromanganese production—lessons learnt from pilot-scale test work, in: TMS Annual Meeting & Exhibition, Springer Nature Switzerland, Cham, 2023, February, pp. 237–252.
[74] M. Mensah, A. Das, Metallurgical resource recovery from waste steelmaking slag from electric arc furnace, Environ. Technol. 44 (2) (2023) 260–277.
[75] M. Shahabuddin, G. Brooks, M.A. Rhamdhani, Decarbonisation and hydrogen integration of steel industries: recent development, challenges and technoeconomic analysis, J. Clean. Prod. (2023) 136391.
[76] A. Kandalam, M.A. Reuter, M. Stelter, M. Reinmöller, M. Gräbner, A. Richter, A. Charitos, A review of top submerged lance (TSL) processing—Part II: thermodynamics, slag chemistry and plant flowsheets, Metals 13 (10) (2023) 1742.
[77] A. Belabid, H. Akhzouz, H. Elminor, H. Elminor, Characteristics of traditional building materials and techniques based on earth, stone and timber: an overview and focus on Morocco, J. Eng. 10 (3) (2023).
[78] Y. Bao, S. Li, Y. Pei, Practical research on external space design of primary and secondary schools in damp and hot areas, Journal of Civil Engineering and Urban Planning 5 (8) (2023) 16–23.
[79] M. Kirschen, V. Risonarta, H. Pfeifer, Energy efficiency and the influence of gas burners to the energy related carbon dioxide emissions of electric arc furnaces in steel industry, Energy 34 (9) (2009) 1065–1072.
[80] J. Dock, Pathways to Climate-Neutral EAF Steel Production Based on Energy Efficiency and Integration of Renewable Energy, 2023.
[81] B. Gajdzik, W. Sroka, J. Vveinhardt, Energy intensity of steel manufactured utilising EAF technology as a function of investments made: the case of the steel industry in Poland, Energies 14 (16) (2021) 5152.
[82] L.G. Carmona, K. Whiting, A. Carrasco, T. Sousa, The evolution of resource efficiency in the United Kingdom's steel sector: an exergy approach, Energy Convers. Manag. 196 (2019) 891–905.
[83] E. Hoikkaniemi, *Use Of Biochar as a Slag Foaming Agent in EAF Steelmaking* (Master's Thesis, E. Hoikkaniemi), 2022.
[84] F. Andersson, Integrating Biomass Gasification with Electric Arc Furnace Steel Making, 2023.
[85] A. Andersson, J. Isaksson, A. Lennartsson, F. Engström, Insights into the valorization of Electric Arc Furnace slags as supplementary cementitious materials, Journal of Sustainable Metallurgy 10 (1) (2024) 96–109.
[86] Q. Luo, Y. Chen, S. Abraham, Y. Wang, R. Petty, A.K. Silaen, C. Zhou, Effects of EAF operations on water-cooling panel overheating, Steel Res. Int. 93 (9) (2022) 2100844.
[87] M.M. Elkoumy, A.M. Fathy, G.M. Megahed, I. El-Mahallawi, H. Ahmed, M. El-Anwar, Empirical model for predicting process parameters during Electric Arc Furnace refining stage based on real measurements, Steel Res. Int. 90 (11) (2019) 1900208.
[88] M. Elkoumy, M. El-Anwar, A. Fathy, G. Megahed, I. El-Mahallawi, H. Ahmed, Computational simulation model for metallurgical effects during EAF refining stage: waiting and arcing time, ISIJ Int. 58 (9) (2018) 1669–1678.
[89] M.M. Elkoumy, M. El-Anwar, A.M. Fathy, G.M. Megahed, I. El-Mahallawi, H. Ahmed, Simulation of EAF refining stage, Ain Shams Eng. J. 9 (4) (2018) 2781–2793.
[90] P. Wiboonchutikula, B. Chaivichayachat, J. Chontanawat, Sources of energy intensity change of Thailand's Steel industry in the decade of global turbulent time, Singapore Econ. Rev. 59 (3) (2014) 1450027.
[91] S. Dasgupta, J. Roy, Analysing energy intensity trends and decoupling of growth from energy use in Indian manufacturing industries during 1973–1974 to 2011–2012, Energy Efficiency 10 (4) (2017) 925–943.
[92] E. Chan, M. Riley, T. Mj, E. Ej, Nitrogen oxides (NOx) formation and control in an electric arc furnace (EAF): analysis with measurements and computational fluid dynamics (CFD) modeling, ISIJ Int. 44 (2) (2004) 429–438.
[93] G.A. Irons, Developments in electric arc furnace steelmaking, in: AISTECH-CONFERENCE PROCEEDINGS, vol. 1, Association for Iron & Steel Technology, 2005, p. 3.
[94] A. Fathi, Y. Saboohi, I. Škrjanc, V. Logar, Comprehensive Electric Arc Furnace model for simulation purposes and model-based control, Steel Res. Int. 88 (3) (2017) 1600083.
[95] R.D. MacRosty, C.L. Swartz, Dynamic modeling of an industrial electric arc furnace, Ind. Eng. Chem. Res. 44 (21) (2005) 8067–8083.
[96] S. Shyamal, C.L. Swartz, Real-time energy management for electric arc furnace operation, J. Process Control 74 (2019) 50–62.
[97] G. Ojp, M.A. RamíRez-Argáez, C. An, Effect of arc length on fluid flow and mixing phenomena in AC electric arc furnaces, ISIJ Int. 50 (1) (2010) 1–8.
[98] S. Jlg, C. An, R.A. Ma, Effect of foamy slag height on hot spots formation inside the electric arc furnace based on a radiation model, ISIJ Int. 52 (5) (2012) 804–813.
[99] J.C. Gruber, T. Echterhof, H. Pfeifer, Investigation on the influence of the arc region on heat and mass transport in an EAF freeboard using numerical modeling, Steel Res. Int. 87 (1) (2016) 15–28.
[100] G. Wei, R. Zhu, K.A.I. Dong, G. Ma, T. Cheng, Research and analysis on the physical and chemical properties of molten bath with bottom-blowing in EAF steelmaking process, Metall. Mater. Trans. B 47 (2016) 3066–3079.
[101] S.C. Koria, K.W. Lange, A new approach to investigate the drop size distribution in basic oxygen steelmaking, Metall. Trans. A B 15 (1984) 109–116.
[102] H.J. Odenthal, A. Kemminger, F. Krause, L. Sankowski, N. Uebber, N. Vogl, Review on modeling and simulation of the electric arc furnace (EAF), Steel Res. Int. 89 (1) (2018) 1700098.
[103] A. Rafiee, K.R. Khalilpour, D. Milani, M. Panahi, Trends in CO2 conversion and utilization: a review from process systems perspective, J. Environ. Chem. Eng. 6 (5) (2018) 5771–5794.
[104] M.N. Al-Harbi, S.K. Mishra, M. Maity, S. Al-Turky, 15thMETEC &InSteelCon, Düsseldorf, Germany, 2011, p. 1.